TIME-DISTANCE HELIOSEISMOLOGY: THE FORWARD PROBLEM FOR RANDOM DISTRIBUTED SOURCES

L. GIZON AND A. C. BIRCH

W. W. Hansen Experimental Physics Laboratory, Stanford University, Stanford, CA 94305

ABSTRACT

The forward problem of time-distance helioseismology is computing travel-time perturbations that result from perturbations to a solar model. We present a new and physically motivated general framework for calculations of the sensitivity of travel times to small local perturbations to solar properties, taking into account the fact that the sources of solar oscillations are spatially distributed. In addition to perturbations in sound speed and flows, this theory can also be applied to perturbations in the wave excitation and damping mechanisms. Our starting point is a description of the wave field excited by distributed random sources in the upper convection zone. We employ the first Born approximation to model scattering from local inhomogeneities. We use a clear and practical definition of travel-time perturbation, which allows a connection between observations and theory. In this framework, travel-time sensitivity kernels depend explicitly on the details of the measurement procedure. After developing the general theory, we consider the example of the sensitivity of surface gravity wave travel times to local perturbations in the wave excitation and damping rates. We derive explicit expressions for the two corresponding sensitivity kernels. We show that the simple single-source picture, employed in most time-distance analyses, does not reproduce all of the features seen in the distributed-source kernels developed in this paper.

Subject headings: scattering — Sun: helioseismology — Sun: interior — Sun: oscillations — waves

1. INTRODUCTION

Time-distance helioseismology, introduced by Duvall et al. (1993b), has yielded numerous exciting insights into the interior of the Sun. This technique, which gives information about travel times for wave packets moving between any two points on the solar surface, is an important complement to global-mode helioseismology, as it is able to probe subsurface structure and dynamics in three dimensions. Some of the main results concern flows and wave-speed perturbations underneath sunspots (Duvall et al. 1996; Kosovichev, Duvall, & Scherrer 2000; Zhao, Kosovichev, & Duvall 2001), large-scale subsurface poleward flows (Giles et al. 1997), and supergranulation flows (Duvall & Gizon 2000).

The interpretation of time-distance data can be divided into a forward and an inverse problem. The forward problem is to determine the relationship between the observational data (travel times $\delta\tau$) and internal properties (q_α). Generally, this relationship is sought in the form of a linear integral equation,

$$\delta\tau = \sum_\alpha \int_\odot d\boldsymbol{r}\, \delta q_\alpha(\boldsymbol{r}) K^\alpha(\boldsymbol{r}) , \qquad (1)$$

where the $\delta q_\alpha(\boldsymbol{r})$ represent the deviations in internal solar properties from a theoretical reference model. The index α refers to all relevant types of independent perturbations, such as sound speed, flows, or magnetic field. The integral $\int_\odot d\boldsymbol{r}$ denotes spatial integration over the volume of the Sun. The kernels of the integrals, $K^\alpha(\boldsymbol{r})$, give the sensitivity of travel times to the perturbations to the solar model. The inverse problem is to invert the above equation, i.e., to estimate δq_α, as a function of position $\boldsymbol{r}$, from the observed $\delta\tau$. In this paper we consider only the forward problem.

An accurate solution to the forward problem is necessary for making quantitative inferences about the Sun from time-distance data. There have been a number of previous efforts to understand the effect of local perturbations on travel times. D'Silva et al. (1996), Kosovichev (1996), and Zhao et al. (2001) used geometrical acoustics to describe the interaction of acoustic waves with sound-speed perturbations and flows. Bogdan (1997) argued that a finite-wavelength theory is needed. Birch & Kosovichev (2000) solved the linear forward problem for sound-speed perturbations, in the single-source approximation. Jensen, Jacobsen, & Christensen-Dalsgaard (2000) solved a weakly nonlinear forward problem for sound-speed perturbations, in the single-source approximation, and proposed the use of Fresnel-zone–based travel-time kernels. Bogdan, Braun, & Lites (1998) used a normal mode approach to compute travel-time perturbations in a model sunspot. Woodard (1997) estimated the effect of wave absorption by sunspots on travel times. This important work, which required a model for random distributed wave sources, is one of the primary motivations for obtaining a general theory for travel-time sensitivity kernels. The model developed by Woodard (1997) employs, however, the approximation that wave damping affects only the amplitude of transmitted waves, ignoring scattering. Birch et al. (2001) tested the accuracy of travel times obtained in the Born approximation, which models single scattering from local inhomogeneities. Although the above-mentioned efforts represent substantial progress, there is not yet a general procedure for relating actual travel-time measurements to perturbations to a solar model that takes into account random distributed sources for solar oscillations, despite a preliminary study by Gizon & Birch (2001).

The first part of this paper (§ 2) is an attempt to synthesize and extend the current knowledge into a flexible framework for the computation of the linear sensitivity of travel times to local inhomogeneities. We start from a physical description of the wave field, including wave excitation and damping. We incorporate the details of the measurement

procedure. Two other key ingredients of our approach are the single-scattering Born approximation and a clear observational definition of travel time, both taken from the geophysics literature (e.g., Tong et al. 1998; Zhao & Jordan 1998; Marquering, Dahlen, & Nolet 1999). The main difference between the geophysics and helioseismology problems is that helioseismology deals with multiple random wave sources as opposed to a single isolated source.

The second part of this paper (§ 3) is an example calculation of travel time kernels for surface gravity waves. The purpose is to demonstrate the application of the general theory described in § 2. We compute travel-time kernels for local perturbations in source strength and damping rate. In our model, these perturbations are confined to the surface and therefore are computationally convenient, as we obtain two-dimensional kernels. Localized source and damping perturbations are interesting and not yet well understood. For this example, we also compare these kernels with kernels calculated in the single-source picture (Birch & Kosovichev 2000; Jensen et al. 2000), in which distributed random sources are replaced by an artificial causal source placed at one of the observation points. We show that the single-source kernels do not reproduce all the features seen in the distributed-source kernels.

2. GENERAL THEORY

2.1. *Definition of Travel Times*

The fundamental data of modern helioseismology are high-resolution Doppler images of the Sun's surface. In general, the filtered line-of-sight projection of the velocity field can be written as

$$\phi = \mathscr{F}\left\{\hat{\boldsymbol{l}} \cdot \boldsymbol{v}\right\}, \qquad (2)$$

where $\boldsymbol{v}$ is the Eulerian velocity and $\hat{\boldsymbol{l}}$ is a unit vector in the direction of the line of sight. The operator $\mathscr{F}$ describes the filter used in the data analysis, which includes the time window (time duration T), instrumental effects, and other filtering.

The basic computation in time-distance helioseismology is the temporal cross-correlation, $C(\mathbf{1}, \mathbf{2}, t)$, between the signal, ϕ, measured at two points, $\mathbf{1}$ and $\mathbf{2}$, on the solar surface,

$$C(\mathbf{1}, \mathbf{2}, t) = \frac{1}{T} \int_{-\infty}^{\infty} dt' \, \phi(\mathbf{1}, t') \phi(\mathbf{2}, t' + t), \qquad (3)$$

where T is the time duration of the observation. The cross-correlation is useful, since it is a phase-coherent average of inherently random oscillations. It can be seen as a solar seismogram, providing information about travel times, amplitudes, and the shape of the wave packets traveling between any two points on the solar surface. Figure 1 shows an example of a surface gravity wave cross-correlation. The positive-time branch corresponds to waves moving from $\mathbf{1}$ to $\mathbf{2}$, and the negative-time branch represents waves moving in the opposite direction. For acoustic waves there are additional branches, at larger absolute time, corresponding to multiple bounces off the surface in between $\mathbf{1}$ and $\mathbf{2}$.

We define the "travel time" for each branch to be the time lag that minimizes the difference between the measured cross-correlation, C, and a sliding reference wavelet, C^{ref}. Depending on the choice of reference wavelet, the term "travel time" may be an abuse of language; this issue will be clarified later. The travel time for waves going from $\mathbf{1}$ to $\mathbf{2}$
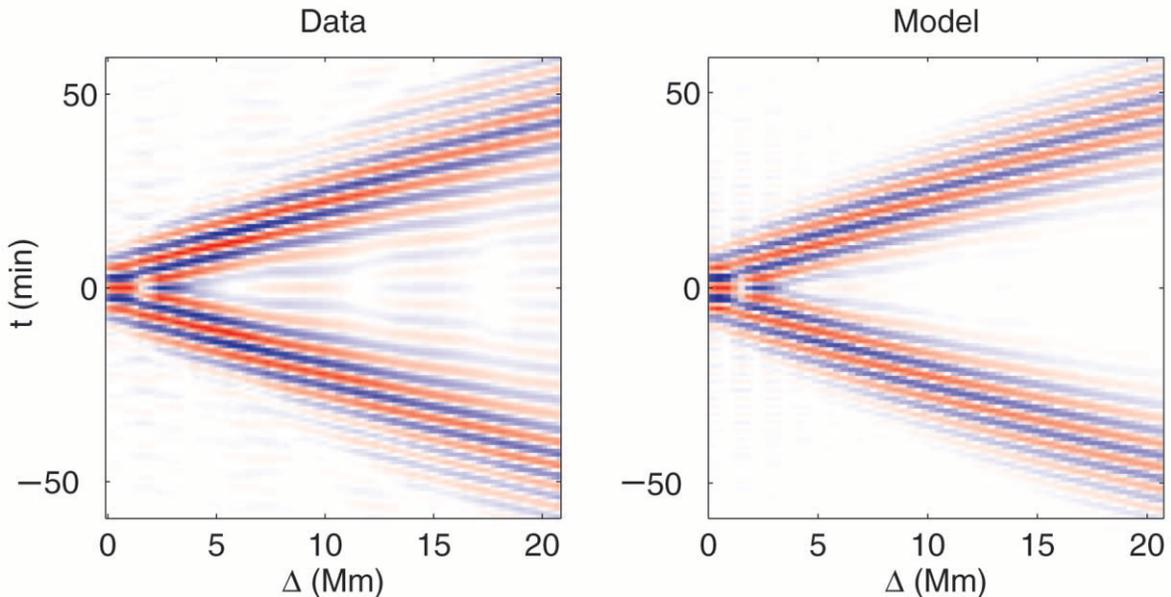
FIG. 1.—Surface gravity wave cross-correlations. *Left*: Example of an observed cross-correlation $C(\mathbf{1}, \mathbf{2}, t)$ averaged over all possible pairs of points $(\mathbf{1}, \mathbf{2})$, as a function of distance $\Delta = \|\mathbf{2} - \mathbf{1}\|$ and time t. Red refers to positive values and blue to negative values. The observations are 8 hr time series from the MDI/*SOHO* high-resolution field of view (Scherrer et al. 1995). The filter $\mathscr{F}$ is chosen to isolate surface gravity waves around 3 mHz. This spatially averaged cross-correlation could be used as the reference wavelet C^{ref}, which is used to measure travel times (see § 2.1). *Right*: Theoretical cross-correlation from the model discussed in § 3.

is denoted by $\tau_+(\mathbf{1},\ \mathbf{2})$, and the travel time for waves going from **2** to **1** by $\tau_-(\mathbf{1},\ \mathbf{2})$. The difference (in the least-squares sense) between the observed cross-correlation and the reference wavelet is

$$
X_\pm(\mathbf{1},\ \mathbf{2},\ t) = \int_{-\infty}^{\infty} dt'\, f(\pm t')
$$
$$
\times \left[C(\mathbf{1},\ \mathbf{2},\ t') - C^{\mathrm{ref}}(\mathbf{1},\ \mathbf{2},\ t' \mp t) \right]^2 . \quad (4)
$$

The window function, $f(t')$, is a one-sided function (zero for t' negative) used to separately examine the positive- and negative-time parts of the cross-correlation. The window $f(t')$ is used to measure τ_+, and $f(-t')$ is used to measure τ_-. One possible choice is a window that isolates the first-skip branch of the cross-correlation. Other window functions could be chosen to, for example, isolate the second-bounce branch of a cross-correlation in the case of acoustic modes.

By definition, the travel times $\tau_\pm$ are the time lags that minimize $X_\pm$:

$$
\tau_\pm(\mathbf{1},\ \mathbf{2}) = \arg\min_t \{ X_\pm(\mathbf{1},\ \mathbf{2},\ t) \} . \quad (5)
$$

Minimizing $X_\pm$ is equivalent to fitting $C^{\mathrm{ref}}(t' \mp t)$ to $C(t')$ with a weighting in time given by $f(\pm t')$, varying the time lag t only. An example of measuring the travel times $\tau_\pm$ from a cross-correlation is shown in Figure 2.

The choice of reference wavelet $C^{\mathrm{ref}}(\mathbf{1},\ \mathbf{2},\ t)$ is left to the observer. For most applications the reference wavelet need only be a function of distance $\Delta = \|\mathbf{2} - \mathbf{1}\|$ and time t. As was done in Figure 2, one possible choice is to take C^{ref} to look like a cross-correlation. In this case, τ_+ and τ_- are

small and the term "travel time" should be understood to mean "time lag." A reference wavelet that resembles a cross-correlation can be constructed by either averaging the observed cross-correlations over all possible pairs of points $(\mathbf{1}, \mathbf{2})$ for each distance Δ (see Fig. 1), or by computing a theoretical cross-correlation from a solar model (see § 3). Another possible choice is to take $C^{\mathrm{ref}}(\mathbf{1},\ \mathbf{2},\ t)$ to look like a single wavelet centered about $t = 0$. In this case τ_+ and τ_- will essentially represent the time it takes for wave packets to travel between the observation points, and the denomination "travel times" for $\tau_\pm$ is appropriate.

The definition of travel time presented here is analogous to the typical definition of travel time used in the geophysics literature (e.g., Zhao & Jordan 1998). In time-distance helioseismology, Duvall et al. (1997) measure travel times by fitting a Gaussian wavelet to cross-correlations. This procedure distinguishes between group and phase travel times, by allowing both the envelope and the phase of the wavelet to vary independently. Our definition is a simplification of this procedure, as it contains only one travel-time parameter per branch. The travel time defined here is neither a pure group or phase time; it is, however, perfectly well defined and has already been used in a time-distance study with real data (Gizon, Duvall, & Larsen 2000). Without significant difficulty, the fitting presented here could be extended to include more parameters, for example amplitude and central frequency, as is done by Duvall et al. (1997).

Traditionally, mean and difference travel times have been used in place of the one-way travel times. The mean and dif-
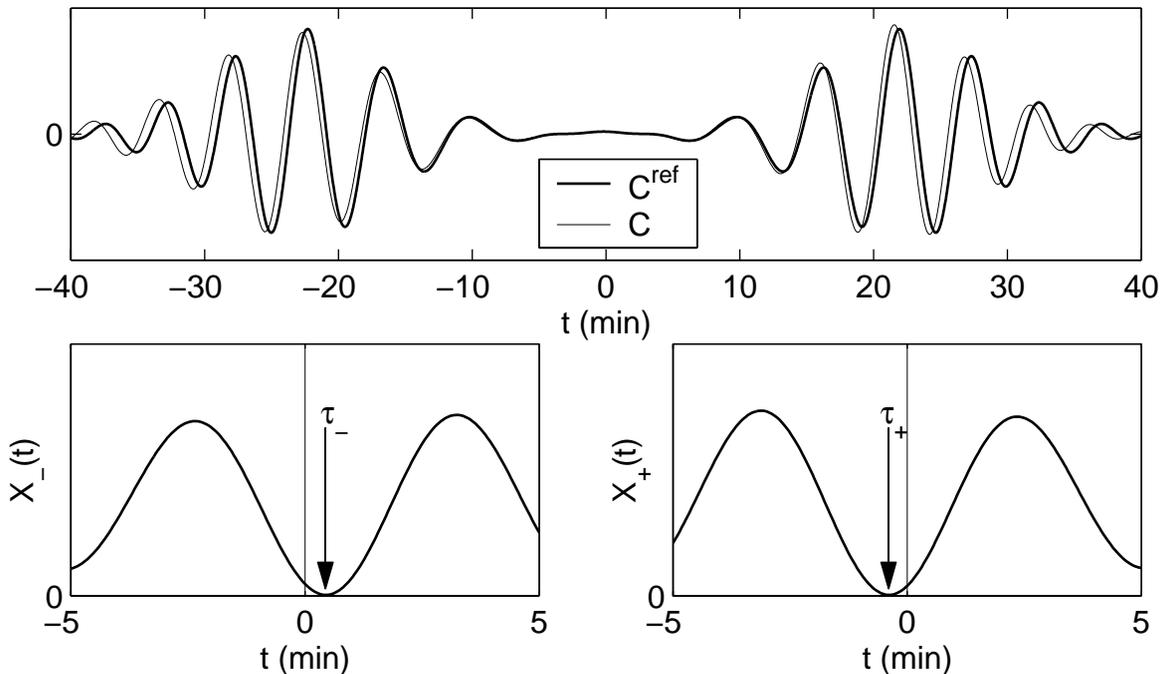
FIG. 2.—Example showing how to measure the travel times $\tau_\pm$ from a cross-correlation $C(\mathbf{1}, \mathbf{2}, t)$. In this figure we choose the reference wavelet C^{ref} (*top panel, heavy line*) to be the zero-order cross-correlation, for the distance $\Delta = 10$ Mm, from the surface gravity wave example discussed in § 3. In general, the observer is free to choose any reference wavelet. This function C^{ref} is even in time. The light line (*top panel*) shows an example cross-correlation, C, which in this particular case was computed from a model including a uniform horizontal flow of 400 m s^{-1} in the direction $\mathbf{1} \rightarrow \mathbf{2}$. To measure the travel times $\tau_\pm$ from C we need to minimize the functions $X_\pm$. The bottom panels show the functions $X_-(t)$ and $X_+(t)$, constructed using eq. (4). The window function f was chosen to be the Heaviside step function. For the positive-time branch of C, the best fit is obtained by shifting C^{ref} toward $t = 0$ (to the left). The minimum of $X_+(t)$ occurs at a negative time τ_+, as can be seen in the bottom right panel. For the negative-time branch of C, the minimum of the function $X_-(t)$ occurs at a positive time τ_- (see bottom left panel). The locations, τ_- and τ_+, of the minima of the functions $X_-(t)$ and $X_+(t)$ are, by definition, the measured travel times. In this particular example the signs $\tau_+ < 0$ and $\tau_- > 0$ make sense, since waves travel faster with the flow than against it.

ference travel times are obtained from the one-way travel times by

$$\tau_{\text{mean}} = \tfrac{1}{2}(\tau_+ + \tau_-) \,, \qquad (6)$$

$$\tau_{\text{diff}} = \tau_+ - \tau_- \,. \qquad (7)$$

The motivation behind using τ_{mean} and τ_{diff} is that sound-speed perturbations are expected to contribute mostly to the mean travel time and flows to the travel-time difference (e.g., Kosovichev & Duvall 1998).

The definition of travel-time perturbations described here leaves observers free to measure without reference to a solar model. We note, however, that in order for a proper interpretation of measured travel-time perturbations to be made it is essential for observers to report their choices of reference wavelet C^{ref}, window function f, and filter $\mathscr{F}$. A solar model is only necessary for the next step, the interpretation of travel-time perturbations in terms of local perturbations to a solar model, to which we now turn.

2.2. Interpretation of Travel Times

The goal of time-distance helioseismology is to estimate the internal solar properties that produce model travel times that best match observed travel times. To achieve this, we need to know how to compute the travel times for a particular solar model. In order to make the inverse problem feasible, we also need to linearize the forward problem around a background state that is close to the Sun.

A background solar model is fully specified by a set of internal properties (density, pressure, etc.), which we denote by $q_\alpha(\boldsymbol{r})$ for short. Standard solar models provide a reasonable background state. In the background state the cross-correlation and the travel times are C^0 and $\tau_\pm^0$, respectively. We then consider small perturbations, $\delta q_\alpha(\boldsymbol{r})$, to the solar properties. These perturbations could include, for example, local changes in density, sound speed, or flows. The difference between the resulting cross-correlation, C, and the background cross-correlation we denote by δC,

$$\delta C(\boldsymbol{1}, \ \boldsymbol{2}, \ t) = C(\boldsymbol{1}, \ \boldsymbol{2}, \ t) - C^0(\boldsymbol{1}, \ \boldsymbol{2}, \ t) \,. \qquad (8)$$

Likewise, the perturbed travel times $\delta\tau_\pm$ are

$$\delta\tau_\pm(\boldsymbol{1}, \ \boldsymbol{2}) = \tau_\pm(\boldsymbol{1}, \ \boldsymbol{2}) - \tau_\pm^0(\boldsymbol{1}, \ \boldsymbol{2}) \,. \qquad (9)$$

The travel times $\tau_\pm(\boldsymbol{1}, \ \boldsymbol{2})$ are measured from the cross-correlation $C(\boldsymbol{1}, \ \boldsymbol{2}, \ t)$. The reference times $\tau_\pm^0$ are the travel times that would be measured if the Sun and the background model were identical.

Since we are considering small changes in the solar model, the correction to the model cross-correlation, δC, will also be small. As a result, we can linearize the dependence of the travel-time perturbations $\delta\tau_\pm$ on δC. The algebra is detailed in Appendix A. The result of this calculation can be written as

$$\delta\tau_\pm(\boldsymbol{1}, \ \boldsymbol{2}) = \int_{-\infty}^{\infty} dt \, W_\pm(\boldsymbol{1}, \ \boldsymbol{2}, \ t)\delta C(\boldsymbol{1}, \ \boldsymbol{2}, \ t) \,. \qquad (10)$$

The functions $W_\pm$ depend on the zero-order cross-correlation C^0, the reference wavelet C^{ref}, and the window function f, and are given in equation (A7). The sensitivity of $\delta\tau_\pm$ to δC is given by the weight functions $W_\pm$. We emphasize that the travel-time perturbations $\delta\tau_\pm$ are proportional to δC, which is a first-order perturbation to the background solar model. We interpret the right-hand side of equation (10) as a model for the difference between the observed travel times

and the theoretical travel times in the background solar model.

The source of solar oscillations is turbulent convection near the solar surface (e.g., Stein 1967). As a result, the signal ϕ and the cross-correlation C are realizations of a random process. In general, a random variable is fully characterized by its expectation value and all of its higher order moments. As a result, to describe a travel-time perturbation $\delta\tau$ we need its expectation value (ensemble average) as well as its variance, etc. In this paper we consider only the expectation value. A calculation of the variance of the travel times would be essential to characterize the realization noise in travel time measurements. An accurate estimate of the noise in travel time measurements is important for solving the inverse problem.

In this paper we only compute the expectation values of travel-time perturbations and cross-correlations. This represents a first and necessary step. Note in addition that under the assumptions of the Ergodic theorem (e.g., Yaglom 1962) the cross-correlations (hence travel times) tend to their expectation values as the observational time interval increases.

2.3. Modeling the Observed Signal

In order to obtain the cross-correlation, C^0, and its first-order perturbation, δC, we need to compute the observable, ϕ, defined in equation (2), and therefore the wave velocity $\boldsymbol{v}$. Linear oscillations are governed by an equation of the form (e.g., Gough 1993)

$$\mathscr{L}\boldsymbol{v} = \boldsymbol{S} \,. \qquad (11)$$

The vector $\boldsymbol{S}$ denotes the source of excitation for the waves. The linear operator $\mathscr{L}$, acting on $\boldsymbol{v}$, should encompass all the physics of wave propagation in an inhomogeneous stratified medium permeated by flows and magnetic fields. Damping processes should also be accounted for in $\mathscr{L}$. An explicit expression for the operator $\mathscr{L}$ including steady flows is provided by Lynden-Bell & Ostriker (1967). Bogdan (2000) includes magnetic field.

We now expand $\mathscr{L}$, $\boldsymbol{v}$, and $\boldsymbol{S}$ into zero- and first-order contributions, which refer to the background solar model and to the lowest order perturbation to that model:

$$\mathscr{L} = \mathscr{L}^0 + \delta\mathscr{L} \,, \qquad (12)$$

$$\boldsymbol{v} = \boldsymbol{v}^0 + \delta\boldsymbol{v} \,, \qquad (13)$$

$$\boldsymbol{S} = \boldsymbol{S}^0 + \delta\boldsymbol{S} \,. \qquad (14)$$

The operator $\delta\mathscr{L}$ depends on first-order quantities such as local perturbations in density, sound speed, and damping rate, as well as flows and magnetic field. In general, one can contemplate time-dependent perturbations. There are, however, many interesting structures on the Sun (e.g., supergranules, meridional flow, moat flows) that are approximately time independent on the timescale on which time-distance measurements are made (at least several hours). As a result, for the sake of simplicity, we only consider time-independent perturbations. These perturbations, which we denote by $\delta q_\alpha(\boldsymbol{r})$ for short, are thus only functions of position $\boldsymbol{r}$ in the solar interior.

To lowest order, equation (11) reduces to

$$\mathscr{L}^0\boldsymbol{v}^0 = \boldsymbol{S}^0 \,. \qquad (15)$$

In order to solve this equation, we introduce a set of causal

Green's vectors G^i defined by

$$\mathcal{L}^0 G^i(x, t; s, t_s) = \hat{e}_i(s)\delta_{\mathrm{D}}(x - s)\delta_{\mathrm{D}}(t - t_s), \quad (16)$$

where the $\hat{e}_i(s)$ are three orthogonal basis vectors at the point s, and δ_{D} is the Dirac delta function. The vector $G^i(x, t; s, t_s)$ is the velocity at location x and time t that results from a unit impulsive source in the $\hat{e}_i$ direction at time t_s and location s. Note that the vector G^i does not in general point in the direction of $\hat{e}_i$. Guided by equation (2), we define the zero-order Green's functions for the observable ϕ:

$$\mathcal{G}^i(x, t; s, t_s) = \mathcal{F}\left\{\hat{l}(x) \cdot G^i(x, t; s, t_s)\right\}. \quad (17)$$

In terms of $\mathcal{G}^i$, the unperturbed signal reads

$$\phi^0(x, t) = \int_\odot ds \int_{-\infty}^{\infty} dt_s\, \mathcal{G}^i(x, t; s, t_s) S_i^0(s, t_s). \quad (18)$$

The sum is taken over the repeated index i, as is done for all repeated indexes throughout this paper.

To the next order of approximation, equation (11) gives

$$\mathcal{L}^0 \delta v = -\delta\mathcal{L} v^0 + \delta S. \quad (19)$$

This is the single-scattering Born approximation (e.g., Sakurai 1995). The first-order Born approximation has been shown to work for small perturbations (e.g., Hung, Dahlen, & Nolet 2000; Birch et al. 2001). We note that equation (19) is of the same form as equation (15): the term $-\delta\mathcal{L} v^0 + \delta S$ appears as a source for the scattered wave velocity δv. The solution to equation (19) is thus

$$\delta v(x, t) = \int_\odot ds \int_{-\infty}^{\infty} dt_s\, G^i(x, t; s, t_s)$$
$$\times \left\{-\delta\mathcal{L} v^0(s, t_s) + \delta S(s, t_s)\right\}_i, \quad (20)$$

where $\{\ldots\}_i$ denotes the ith component of the vector inside the curly braces.

By expressing the zero-order velocity v^0 in terms of the Green's function and the source, and using equation (20) and $\delta\phi = \mathcal{F}\{\hat{l} \cdot \delta v\}$, the perturbed signal can be written as

$$\delta\phi(x, t) = \left[\int_\odot dr \int_{-\infty}^{\infty} dt' \int_\odot ds \int_{-\infty}^{\infty} dt_s\, \mathcal{G}^i(x, t; r, t')\right.$$
$$\left.\times \left\{-\delta\mathcal{L} G^j(r, t'; s, t_s)\right\}_i S_j^0(s, t_s)\right]$$
$$+ \int_\odot ds \int_{-\infty}^{\infty} dt_s\, \mathcal{G}^i(x, t; s, t_s)\delta S_i(s, t_s). \quad (21)$$

We recall that the operator $\delta\mathcal{L}$ contains the first-order perturbations to the solar model, $\delta q_\alpha(r)$. The first term in the above equation contains two Green's functions; it represents the contribution to $\delta\phi(x, t)$ that comes from a wave that is created by the source at location s at time t_s, is scattered at time t' by the perturbations at location r, and then propagates to the location x. The details of the scattering process are encoded in the operator $\delta\mathcal{L}$. The second term results from the perturbation to the source function, and involves only a single Green's function, which propagates waves from the location and time of the source to the observation location and time. As we now have ϕ^0 and $\delta\phi$, we can next compute the zero- and first-order cross-correlations, C^0 and δC.

2.4. *Temporal Cross-Correlation*

We remind the reader that we only want to compute the expectation value of the cross-correlation (see § 2.2). In the rest of this paper, cross-correlations stand for their expectation values. From equation (3) and the equation for ϕ^0 derived in the previous section (eq. [18]), we deduce a general expression for the zero-order cross-correlation:

$$C^0(\mathbf{1},\ \mathbf{2},\ t) = \frac{1}{T}\int dt'\, ds\, dt_s\, ds'\, dt_s'\, M_{ij}^0(s, t_s; s', t_s')$$
$$\times \mathcal{G}^i(\mathbf{1}, t'; s, t_s)\mathcal{G}^j(\mathbf{2}, t' + t; s', t_s'), \quad (22)$$

with

$$M_{ij}^0(s, t_s; s', t_s') = E\left[S_i^0(s, t_s)S_j^0(s', t_s')\right], \quad (23)$$

where $E[\ldots]$ denotes the expectation value of the expression in square brackets. For the sake of readability, we have omitted the limits of integration in equation (23). The matrix M^0 gives the correlation between any two components of S^0, measured at two possibly different positions.

No assumption has been made about M^0 to obtain equation (22). With the assumptions of stationarity in time and homogeneity and isotropy in the horizontal direction, M^0 only depends on the time difference $t_s - t_s'$, the horizontal distance between s and s', and their depths. Further assumptions could be made in order to simplify the computation of equation (22). In the spirit of Woodard (1997), one might assume that the sources are spatially uncorrelated or are located only at a particular depth. A better approach might be to obtain the statistical properties of S^0 from recent numerical simulations of solar convection (e.g., Stein & Nordlund 2000) or observations of photospheric convection (e.g., Title et al. 1989; Chou et al. 1991; Strous, Goode, & Rimmele 2000). Furthermore, a comparison of models and observations of the power spectrum of solar oscillations can be used to constrain the depths and types of sources (e.g., Duvall et al. 1993a).

We now perturb equation (3) and take the expectation value to obtain

$$\delta C(\mathbf{1},\ \mathbf{2},\ t) = \frac{1}{T}\int_{-\infty}^{\infty} dt'\, E\left[\delta\phi(\mathbf{1},\ t')\,\phi^0(\mathbf{2},\ t' + t)\right.$$
$$\left. + \phi^0(\mathbf{1},\ t')\,\delta\phi(\mathbf{2}, t' + t)\right]. \quad (24)$$

The function δC has two contributions, one from the perturbation to the wave operator, $\delta C_\mathcal{L}$, and one from the source perturbation, δC_S:

$$\delta C = \delta C_\mathcal{L} + \delta C_S. \quad (25)$$

Using the expressions for ϕ^0 and $\delta\phi$ given by equations (18) and (21), we obtain the perturbation to the cross-correlation resulting from a change in the wave operator $\mathcal{L}$:

$$\delta C_\mathcal{L}(\mathbf{1},\ \mathbf{2},\ t) = \frac{1}{T}\int dr \int dt'\, dt''\, ds\, dt_s\, ds'\, dt_s'$$
$$\times \left\{-\delta\mathcal{L} G^i(r, t''; s, t_s)\right\}_k M_{ij}^0(s, t_s; s', t_s')$$
$$\times \left[\mathcal{G}^j(\mathbf{2}, t' + t; s', t_s')\, \mathcal{G}^k(\mathbf{1}, t'; r, t'')\right.$$
$$\left. + \mathcal{G}^j(\mathbf{1}, t'; s', t_s')\, \mathcal{G}^k(\mathbf{2}, t' + t; r, t'')\right]. \quad (26)$$

The above equation, which gives the perturbation to the cross-correlation due to scattering, has two components,

illustrated in Figure 3a. The first component comes from the correlation of the scattered wave at **1** with the direct wave at **2**, i.e., $\delta\phi(\mathbf{1}, t')\phi^0(\mathbf{2}, t' + t)$, and the second component comes from $\phi^0(\mathbf{1}, t')\delta\phi(\mathbf{2}, t' + t)$. Both of these components appear in equation (26) as the product of three Green's functions. From the term $\delta\phi(\mathbf{1}, t')\phi^0(\mathbf{2}, t' + t)$ there is one Green's function for the wave that goes directly from $\mathbf{s}'$ to **2**, which gives $\phi^0(\mathbf{2})$. There is a second Green's function for the wave that is created at $\mathbf{s}$ and travels to $\mathbf{r}$, and the third Green's function takes the scattered wave from $\mathbf{r}$ to **1**, which gives $\delta\phi(\mathbf{1})$. The term $\phi^0(\mathbf{1}, t')\delta\phi(\mathbf{2}, t' + t)$ can be understood by switching the roles of **1** and **2**. The scattering process is described by the operator $\delta\mathcal{L}$, which depends on the perturbations $\delta q_\alpha(\mathbf{r})$. The Green's function $\mathcal{G}$ is used for waves that arrive at an observation point as it gives the response of ϕ to a source. The Green's vectors $\mathbf{G}^i$ are used to propagate the wave velocity from a source to the scattering point, as the scattered wave depends on the vector velocity of the incoming wave.

The cross-correlation is also sensitive to changes in the source function. The first-order perturbation resulting from a small change in the source function can be written as (from eqs. [18] and [21])

$$\delta C_S(\mathbf{1}, \; \mathbf{2}, \; t) = \frac{1}{T}\int dt' \, d\mathbf{s} \, dt_s \, d\mathbf{s}' \, dt'_s \, \delta M_{ij}(\mathbf{s}, t_s; \mathbf{s}', t'_s)$$
$$\times \, \mathcal{G}^i(\mathbf{1}, \; t'; \mathbf{s}, t_s)\mathcal{G}^j(\mathbf{2}, \; t' + t; \mathbf{s}', t'_s) \,, \qquad (27)$$

where the perturbation to the source covariance is

$$\delta M_{ij}(\mathbf{s}, t_s; \mathbf{s}', t'_s) = E\Big[S^0_i(\mathbf{s}, t_s) \, \delta S_j(\mathbf{s}', t'_s)$$
$$+ \, \delta S_i(\mathbf{s}, t_s) \, S^0_j(\mathbf{s}', t'_s)\Big] \,. \qquad (28)$$

Figure 3b gives a graphical interpretation of this equation. Unlike the perturbation to the cross-correlation due to scattering, the above equation contains only two Green's functions. One connects the unperturbed source with the unperturbed signal at an observation point, while the second relates the source perturbation to the perturbed signal at the other observation point.

Later in this paper it will be necessary to express the perturbation to the cross-correlation as a spatial integral over the location, $\mathbf{r}$, of the perturbation to the solar model. In
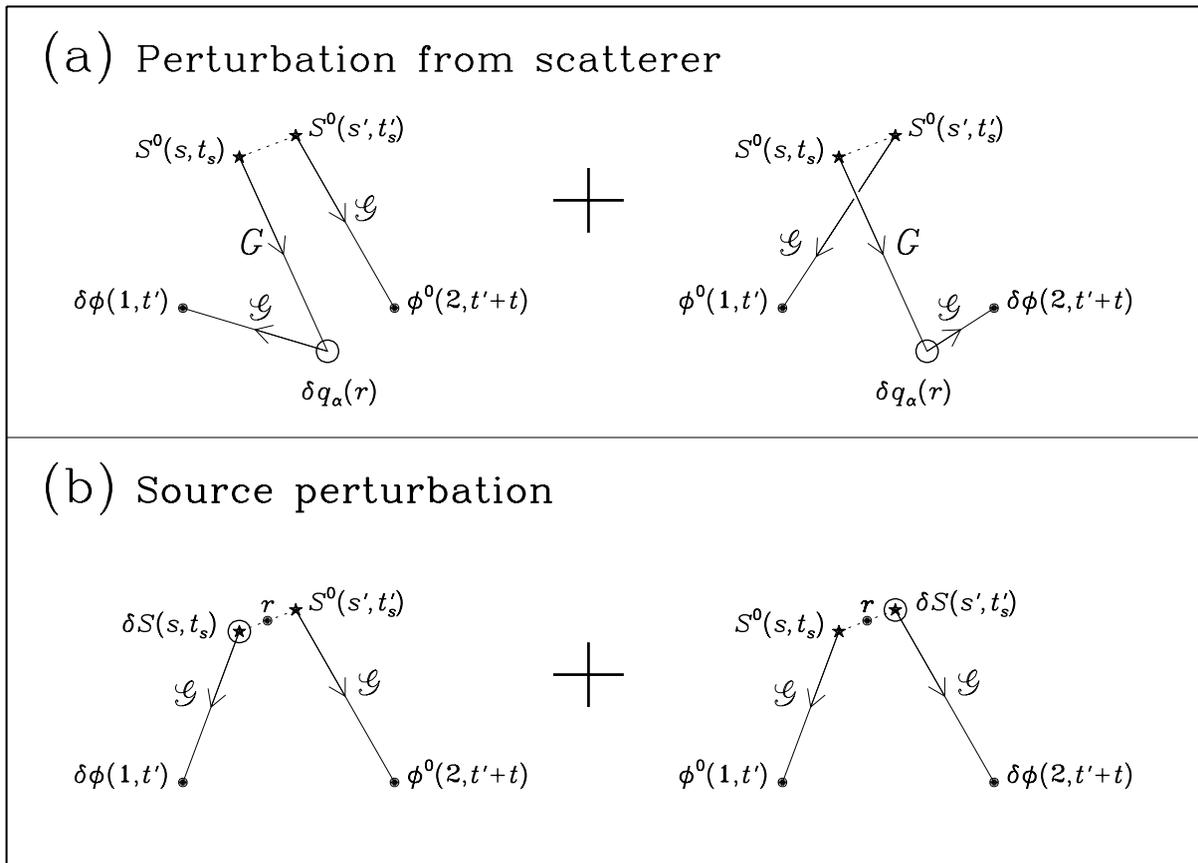
Fig. 3.—Graphical representation of the two types of contributions to the first-order perturbation to the cross-correlation (eqs. [26] and [27]), showing (a) scattering from perturbations $\delta q_\alpha(\mathbf{r})$ to the model and (b) changes δS in the source function. Scattering processes contribute to the cross-correlation as the product of three Green's functions: one Green's function to describe the direct wave from the source to an observation point and two Green's functions to obtain the scattered wave at the other observation point, in the Born approximation. The sensitivity of the cross-correlation to a change in the source function only involves two Green's functions, one to propagate waves from the unperturbed source to an observation point and one to give the response, at the other observation point, to the change in the source function. Throughout the diagram, as in the text, the Green's function for the observable is given by $\mathcal{G}$, and the Green's function for the vector velocity is $\mathbf{G}$. The dotted line between the source locations, $\mathbf{s}$ and $\mathbf{s}'$, indicates that the two sources are connected through the source covariance matrix $\mathbf{M}$.

order to be able to write equation (27) for δC_S in this form, we introduce the change of variable $\boldsymbol{r} = (\boldsymbol{s} + \boldsymbol{s}')/2$ and $\boldsymbol{u} = \boldsymbol{s} - \boldsymbol{s}'$. This change of variable is also useful because we expect the source covariance $\boldsymbol{M}$ to be small for large $\boldsymbol{u}$, i.e., for sources that are far apart. In the limit of very small source correlation length, $\boldsymbol{M}$ is a function only of $\boldsymbol{r}$.

We have shown how to obtain C^0 and δC from an assumed solar model consisting of a background model ($\mathscr{L}^0$ and $\boldsymbol{S}^0$) and small perturbations ($\delta\mathscr{L}$ and $\delta\boldsymbol{S}$). Earlier, in § 2.2, we showed how to connect perturbations to the cross-correlation to travel-time perturbations. In the next section we put these pieces together and obtain travel-time kernels, which give the travel-time perturbations resulting from small changes in the solar model.

2.5. *Travel-Time Sensitivity Kernels*

It is useful for the derivation of travel-time kernels to express the perturbation to the cross-correlation δC as an integral over the location $\boldsymbol{r}$ of the perturbations $\delta q_\alpha(\boldsymbol{r})$. In general, $\delta\mathscr{L}$ and $\delta\boldsymbol{M}$ involve spatial derivatives of the perturbations $\delta q_\alpha(\boldsymbol{r})$ to the solar model, and so integration by parts on the variable $\boldsymbol{r}$ may be required to obtain, from equations (25), (26), and (27),

$$\delta C(\boldsymbol{1},\ \boldsymbol{2},\ t) = \int_\odot d\boldsymbol{r}\, \delta q_\alpha(\boldsymbol{r})\, \mathscr{C}^\alpha(\boldsymbol{1},\ \boldsymbol{2},\ t; \boldsymbol{r})\,. \qquad (29)$$

The index α refers to the different types of perturbations in the solar model, for example, perturbations to sound speed or flows. The sum over α is over all relevant types of perturbations. We note that any particular perturbation δq_α may appear in both the operator $\delta\mathscr{L}$ and the perturbation to the source covariance $\delta\boldsymbol{M}$. For example, a flow will advect waves as well as Doppler shift the sources. For any particular $\delta\boldsymbol{M}(\delta q)$ it may be helpful to do partial integrations on equation (27) before making the change of variable $\boldsymbol{r} = (\boldsymbol{s} + \boldsymbol{s}')/2$ described above. In § 3, we show a detailed example of the derivation of $\mathscr{C}^\alpha$ for local perturbations to source strength and damping rate for surface gravity waves.

In § 2.2 we showed how to relate the travel-time perturbations $\delta\tau_\pm$ to the perturbation to the cross-correlation δC. Using equation (29) for δC and equation (10) for $\delta\tau_\pm$, we obtain

$$\delta\tau_\pm(\boldsymbol{1},\ \boldsymbol{2}) = \int_\odot d\boldsymbol{r}\, \delta q_\alpha(\boldsymbol{r}) \int_{-\infty}^\infty dt\, W_\pm(\boldsymbol{1},\ \boldsymbol{2},\ t)\, \mathscr{C}^\alpha(\boldsymbol{1},\ \boldsymbol{2},\ t; \boldsymbol{r})\,. \qquad (30)$$

Since we want to define sensitivity kernels in the form

$$\delta\tau_\pm(\boldsymbol{1},\ \boldsymbol{2}) = \int_\odot d\boldsymbol{r}\, \delta q_\alpha(\boldsymbol{r}) K_\pm^\alpha(\boldsymbol{1},\ \boldsymbol{2}; \boldsymbol{r})\,, \qquad (31)$$

we make the identification

$$K_\pm^\alpha(\boldsymbol{1},\ \boldsymbol{2}; \boldsymbol{r}) = \int_{-\infty}^\infty dt\, W_\pm(\boldsymbol{1},\ \boldsymbol{2},\ t)\, \mathscr{C}^\alpha(\boldsymbol{1},\ \boldsymbol{2},\ t; \boldsymbol{r})\,. \qquad (32)$$

By definition, $K_\pm^\alpha$ represent the local sensitivity of the travel-time perturbations $\delta\tau_\pm$ to perturbations to the model, δq_α. From the above equation we can see that the kernels depend on both the definition of travel time, through the functions $W_\pm$, and on the zero-order problem and the form of the first-order perturbations, through $\mathscr{C}^\alpha$. The inputs needed to compute $W_\pm$ are the zero-order cross-correlation C^0, and

the reference wavelet C^{ref} and the window function $f(t)$ used in the travel-time measurement procedure (eq. [A7]). The function $\mathscr{C}^\alpha$ depends on the source covariance, the Green's function, the filter, and the forms of the wave operator and the source function (eqs. [26] and [27]).

We have now shown a general procedure for computing travel-time kernels for any particular model. In order to demonstrate the utility and feasibility of this procedure, in the next section we derive two-dimensional kernels for surface gravity waves.

3. AN EXAMPLE: SURFACE GRAVITY WAVES

3.1. *Outline*

In this section we derive the sensitivity of surface gravity wave travel times to local perturbations to source strength and damping rate. We work in a plane-parallel model with constant density and gravity. In this model, wave excitation and attenuation act only at the fluid surface, and the problem can be reduced to a two-dimensional problem. Our model is a very simplified version of the actual solar f-mode case, yet incorporates most of the basic physics. We follow the basic recipe outlined in § 2 for deriving kernels.

The example is written in four parts. In § 3.2 we fully specify the problem: we derive the equations of motion, encapsulated in the operator $\mathscr{L}$, and describe our models for the source covariance and wave damping. We also describe the filter $\mathscr{F}$, which includes an approximation to the MDI/SOHO point-spread function. In § 3.3 we compute the zero-order solution to the problem: the Green's function, power spectrum, and zero-order cross-correlation. Travel-time kernels for perturbations in source strength and damping rate are derived in § 3.4. We conclude, in § 3.5, with a comparison of the kernels from § 3.4 with kernels obtained in the single-source picture.

3.2. *Specification of the Problem*

We consider a simple plane-parallel medium appropriate to studying waves with wavelengths that are small compared to the solar radius. The geometry is shown in Figure 4. The height coordinate is z, measured upward, and a horizontal coordinate vector is denoted by $\boldsymbol{x}$. Gravitational acceleration is assumed to be constant, $-g\hat{\boldsymbol{z}}$, where $g = 274$ m s^{-2} is the solar surface value. For $z < 0$ the fluid has a uniform constant density, ρ. This assumption simplifies the problem considerably and does not affect the dispersion relation ($\omega^2 = gk$). In addition, acoustic waves are not present in this problem because the medium is incompressible. In the steady background state there is a free surface at $z = 0$. The background pressure distribution, $P(z)$, is hydrostatic, with $P = -\rho g z$.

In the following sections, we develop the equations of motion (§ 3.2.1), encapsulated in the operator $\mathscr{L}$, and describe our models for the source covariance (§ 3.2.2) and the wave-damping operator (§ 3.2.3). We also describe the filter $\mathscr{F}$, which includes an approximation to the MDI/SOHO point-spread function (§ 3.2.4). The measurement procedure is specified by choosing the reference wavelet and the window function (§ 3.2.5).

3.2.1. *Equations of Motion*

We now derive the equations of motion, which we want in the form of equation (11). For an inviscid fluid of constant
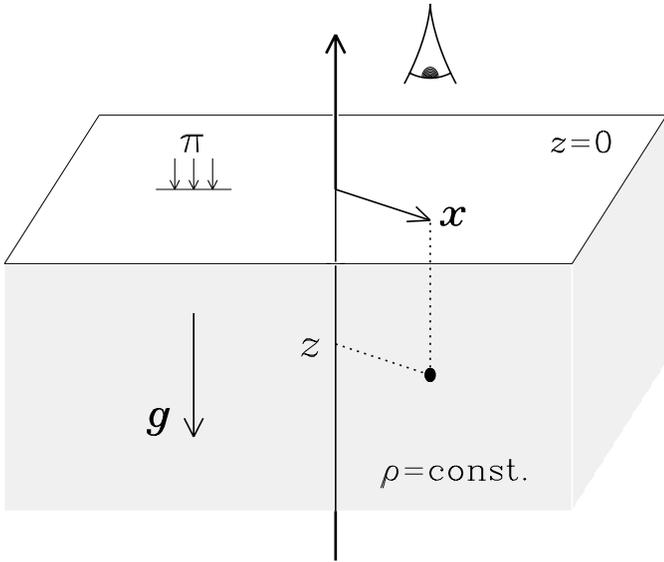
Fig. 4.—Basic setup for the example. The coordinate z denotes height, and x is a horizontal coordinate vector. The half-space $z < 0$ is filled with an incompressible fluid of density ρ, and the space above is empty. The line-of-sight vector is $\boldsymbol{l} = \hat{\boldsymbol{z}}$, i.e., the observer is looking straight down at the surface. Gravitational acceleration is constant and points in the $-\hat{\boldsymbol{z}}$ direction. Surface gravity waves are excited by a stochastic pressure distribution Π applied at the surface, $z = 0$.

density, the linearized equations of conservation of mass and momentum read

$$\nabla \cdot \boldsymbol{v} = 0 \,, \tag{33}$$

$$\rho \dot{\boldsymbol{v}} + \nabla p = 0 \,, \tag{34}$$

where p is the pressure perturbation associated with the waves. Provided that there exists a time at which the velocity field is irrotational, it will remain irrotational for all time. We can imagine a medium free of waves as a starting condition and subsequently switch on the pressure sources at some initial time in the distant past. As a result, we assume that

$$\nabla \times \boldsymbol{v} = 0 \tag{35}$$

holds for all times.

In the Sun, the wave excitation mechanism is near-surface turbulent convection, with various types of sources distributed with depth (e.g., Nigam & Kosovichev 1999; Kumar & Basu 2000). Here, we excite surface gravity waves by applying a stochastic pressure source Π at the fluid surface. Thus, the wave pressure perturbation, p, satisfies the linearized dynamic boundary condition

$$p - \rho g \xi = \Pi, \quad \text{at } z = 0 \,, \tag{36}$$

where ξ is the vertical displacement, which has time derivative equal to the vertical velocity at the surface.

In principle, turbulent convection is also responsible for damping f-modes (e.g., Duvall, Kosovichev, & Murawski 1998). Turbulent convection can also modify the dispersion relation (Murawski & Roberts 1993). Here, however, we use a phenomenological model for wave attenuation by including a dissipative term $\rho \Upsilon \boldsymbol{v}$ in the momentum equation at the surface. The operator Υ is a temporal convolution that reproduces the observed damping rates; it is discussed in detail in § 3.2.3. At the surface, the momentum equation

thus becomes

$$\rho \dot{\boldsymbol{v}} + \nabla p = -\rho \Upsilon \boldsymbol{v}, \quad \text{at } z = 0 \,. \tag{37}$$

Eliminating p from equations (37) and (36), the surface boundary conditions reduce to the equation

$$\partial_z \ddot{w} - g\nabla_h^2 w - \partial_t \nabla_h \cdot (\Upsilon \boldsymbol{u}) = \frac{1}{\rho} \nabla_h^2 \dot{\Pi} \,, \tag{38}$$

where ∇_h is the horizontal gradient and $\boldsymbol{u}$ and w are the horizontal and vertical components of the wave velocity,

$$\boldsymbol{v} = \boldsymbol{u} + w\hat{\boldsymbol{z}} \,. \tag{39}$$

We note that perturbations at the surface do not affect equations (33) and (35) for $z < 0$. As a result, the effect of surface perturbations is contained entirely in equation (38). Therefore, the problem is completely specified by equation (38) on the surface, and the auxiliary equations $\nabla \times \boldsymbol{v} = 0$ and $\nabla \cdot \boldsymbol{v} = 0$ for $z < 0$. The problem is thus essentially two-dimensional, and equation (38) is the relevant equation to put in the form of equation (11). So we have

$$\mathscr{L}\boldsymbol{v} = \partial_z \ddot{w} - g\nabla_h^2 w - \partial_t \nabla_h \cdot (\Upsilon \boldsymbol{u}) \,, \tag{40}$$

$$S = \frac{1}{\rho} \nabla_h^2 \dot{\Pi} \,. \tag{41}$$

We note that the source function S is scalar, unlike in the general theory (§ 2). Now that we have specified the operator $\mathscr{L}$ and the source function S, it remains only to follow the recipe presented in the theory section.

The first part of the recipe is to write the zero-order problem and the first-order Born approximation. We consider two different types of perturbations to the background state: a change in the damping operator, $\delta\Upsilon$, and a change in the source function, δS. The zero-order problem is

$$\mathscr{L}^0 \boldsymbol{v}^0 = S^0 \,, \tag{42}$$

where

$$\mathscr{L}^0 \boldsymbol{v}^0 = \partial_z \ddot{w}^0 - g\nabla_h^2 w^0 + \partial_t \Upsilon^0 \partial_z w^0 \,, \tag{43}$$

$$S^0 = \frac{1}{\rho} \nabla_h^2 \dot{\Pi}^0 \,. \tag{44}$$

Here, S^0 is the zero-order source function, $\mathscr{L}^0$ the zero-order wave operator, and $\boldsymbol{v}^0$ the unperturbed wave velocity. We have used the fact that the zero-order damping operator Υ^0 commutes with spatial derivatives. The first-order approximation gives

$$\mathscr{L}^0 \delta\boldsymbol{v} = -\delta\mathscr{L}\,\boldsymbol{v}^0 + \delta S \,, \tag{45}$$

where

$$-\delta\mathscr{L}\,\boldsymbol{v}^0 = \partial_t \nabla_h \cdot (\delta\Upsilon \boldsymbol{u}^0) \,, \tag{46}$$

$$\delta S = \frac{1}{\rho} \nabla_h^2 \delta\dot{\Pi} \,. \tag{47}$$

Here, δS is the perturbation to the source function, $\delta\mathscr{L}$ the perturbation to the wave operator, and $\delta\boldsymbol{v}$ the first Born approximation to the wave velocity. Note that equation (45) has the same operator, $\mathscr{L}^0$, on the left-hand side as the zero-order problem (eq. [42]).

3.2.2. Source Covariance

In order to model the zero-order covariance M^0 of the source function S^0, which is necessary to compute the cross-correlation, we introduce the covariance of the applied surface pressure distribution Π^0,

$$\rho^2 m^0(\boldsymbol{x}, t; \boldsymbol{x}', t') = E\left[\Pi^0(\boldsymbol{x}, t)\, \Pi^0(\boldsymbol{x}', t')\right], \qquad (48)$$

which is a physical quantity. In terms of m^0, the zero-order source covariance M^0 is given by

$$M^0(\boldsymbol{x}, t; \boldsymbol{x}', t') = \nabla_{\boldsymbol{x}}^2 \nabla_{\boldsymbol{x}'}^2\, \partial_t\, \partial_{t'}\, m^0(\boldsymbol{x}, t; \boldsymbol{x}', t'), \qquad (49)$$

where $\nabla_{\boldsymbol{x}}^2$ denotes the horizontal Laplacian with respect to the variable $\boldsymbol{x}$. Guided by the observations of Title et al. (1989), we write m^0 as a product of spatial and temporal decaying exponentials. Under the assumption of translation invariance (in time and space),

$$m^0(\boldsymbol{x}; t; \boldsymbol{x}', t') = a\, \frac{e^{-\|\boldsymbol{x} - \boldsymbol{x}'\|/L_s}}{2\pi L_s^2}\, \frac{e^{-|t - t'|/T_s}}{2T_s}. \qquad (50)$$

Here L_s is the correlation length and T_s the correlation time of the lowest order turbulent pressure field Π^0. The constant a is the overall amplitude of m^0. The normalization factors $2\pi L_s^2$ and $2T_s$ are included so that in the limits of $L_s \to 0$ and $T_s \to 0$, m^0 becomes the product of two Dirac delta functions, $\delta_{\mathrm{D}}(\boldsymbol{x} - \boldsymbol{x}')$ and $\delta_{\mathrm{D}}(t - t')$.

Title et al. (1989) computed the covariance function of quiet-Sun granulation intensity and found exponential dependence on the temporal and spatial separations, $|t - t'|$ and $\|\boldsymbol{x} - \boldsymbol{x}'\|$, with correlation time 400 s and correlation length 450 km. For this work, we take $T_s = 400$ s and $L_s = 0$. Neglecting the source correlation length, i.e., treating the sources as spatially uncorrelated, is done for the sake of computational simplicity; it is not at all a limitation of the theory. The approximation of zero-correlation length is appropriate because L_s is smaller than a wavelength. For the form of m^0 given by equation (50), and the definition of the Fourier transform appropriate for functions that are translation invariant (eq. [B4]), we obtain

$$m^0(\boldsymbol{k}, \omega) = \frac{a}{(2\pi)^3 [1 + (\omega T_s)^2]}, \quad \text{as } L_s \to 0, \qquad (51)$$

which in particular does not depend on $\boldsymbol{k}$ for spatially uncorrelated sources. Here, as in the rest of the paper, $\boldsymbol{k}$ is the horizontal wavevector and ω is the angular frequency.

We now consider source perturbations. As we have already shown, what matters for the computation of cross-correlations is not the perturbation to the source but rather the perturbed source covariance, δM, which can be obtained from δm through

$$\delta M(\boldsymbol{x}, t; \boldsymbol{x}', t') = \nabla_{\boldsymbol{x}}^2 \nabla_{\boldsymbol{x}'}^2\, \partial_t\, \partial_{t'}\, \delta m(\boldsymbol{x}, t; \boldsymbol{x}', t'). \qquad (52)$$

Three possible types of perturbations to the source covariance are local changes in source correlation time, correlation length, and amplitude. For instance, Title et al. (1989) report different correlation times in the quiet Sun and magnetic network. Magnetic fields affect near-surface convection and thus are expected to introduce local changes in the source strength as well. Here we consider only perturbations to the local amplitude, a, of m, i.e., to model regions of

increased or decreased f-mode emission. We choose

$$\delta m(\boldsymbol{x}, t; \boldsymbol{x}', t') = \frac{\delta a(\boldsymbol{r})}{a}\, m^0(\boldsymbol{x}, t; \boldsymbol{x}', t'), \qquad (53)$$

with

$$\boldsymbol{r} = \tfrac{1}{2}(\boldsymbol{x} + \boldsymbol{x}'). \qquad (54)$$

Here $\delta a(\boldsymbol{r})$ gives the local change in the amplitude of the source covariance. We have used the assumption that the source correlation length is small compared to the length scale of the spatial variation of the amplitude of the source function, to write δa as a function of only the central position $\boldsymbol{r}$.

3.2.3. Damping

Theoretical descriptions of the damping of f-modes by scattering from near-surface convective turbulence exist (e.g., Duvall et al. 1998), but we elect to use a phenomenological model for the sake of simplicity. It is known from observations that high-frequency waves are damped more strongly than low-frequency waves (e.g., Duvall et al. 1998). As a result, we need a frequency-dependent damping rate. The easiest way to implement general frequency dependence is through a temporal convolution (e.g., Dahlen & Tromp 1998). Thus, we express the zero-order damping operator, Υ^0, as

$$\Upsilon^0 \boldsymbol{v}(\boldsymbol{x}, t) = \frac{1}{2\pi} \int_{-\infty}^{\infty} dt'\, \Gamma^0(t - t')\, \boldsymbol{v}(\boldsymbol{x}, t'). \qquad (55)$$

We have assumed that damping is acting purely locally. A more sophisticated model would presumably include a spatial convolution in addition to the temporal convolution. With the Fourier convention given in Appendix B, Υ^0 can be written as

$$\Upsilon^0 \boldsymbol{v}(\boldsymbol{k}, \omega) = \Gamma^0(\omega)\, \boldsymbol{v}(\boldsymbol{k}, \omega), \qquad (56)$$

where $\Gamma^0(\omega)$ is the temporal Fourier transform of $\Gamma^0(t)$. In addition, we see that the operator $\partial_t + \Upsilon^0$, which appears in equation (37), becomes multiplication by $-i\omega + \Gamma^0(\omega)$ in the Fourier domain.

For the sake of simplicity, we choose the function $\Gamma^0(t)$ to be real and even in time. As a result $\Gamma^0(\omega)$ is real and even. A nonphysical consequence of this choice is that the damping operator is not causal. We will see, however, in § 3.3.1, that the Green's function derived using this damping operator is still causal. A treatment of causal frequency-dependent damping can be found in Dahlen & Tromp (1998). In order to damp all frequencies ω, the function $\Gamma^0(\omega)$ must be positive (see § 3.3.1). We will see in § 3.3.2 that $\Gamma^0(\omega)$ is the full frequency width at half-maximum of the surface gravity wave power. We obtain a good fit to observed f-mode line widths (Duvall et al. 1998) if we write $\Gamma^0(\omega)$ in the form

$$\Gamma^0(\omega) = \gamma \left| \frac{\omega}{\omega_*} \right|^{\beta}, \qquad (57)$$

with the parameters $\omega_*/2\pi = 3$ mHz, $\gamma/2\pi = 100$ μHz, and $\beta = 4.4$. This fit is accurate in the range 1.5 mHz $< \omega/2\pi < 5$ mHz. The frequency dependence of the damping rate is strong.

There are two basic types of perturbations to the local damping rate: a change in the amplitude of the damping

rate, γ, and a change in the exponent, β. In this paper we only consider the former and write the perturbation to the damping operator as

$$\delta \Upsilon \, \boldsymbol{v}(\boldsymbol{x}, t) = \frac{\delta \gamma(\boldsymbol{x})}{\gamma} \Upsilon^0 \boldsymbol{v}(\boldsymbol{x}, t) , \qquad (58)$$

where $\delta\gamma(\boldsymbol{x})/\gamma$ is the local fractional perturbation in the damping rate.

3.2.4. Observational Filter

For this example we take the line-of-sight vector to be vertical and independent of horizontal position, $\hat{\boldsymbol{l}} = \hat{\boldsymbol{z}}$. Then in accordance with equation (2) the observable is

$$\phi(\boldsymbol{x}, t) = \mathscr{F}\{\boldsymbol{v}(\boldsymbol{x}, t) \cdot \hat{\boldsymbol{z}}\} . \qquad (59)$$

In this example we consider only the case in which there is no spatial or temporal window function in the filter $\mathscr{F}$, i.e., we observe the wave field over an area A and a time interval T that are both very large. Therefore, the filter $\mathscr{F}$ can be represented by multiplication by a function $F(\boldsymbol{k}, \omega)$ in the Fourier domain,

$$\phi(\boldsymbol{k}, \omega) = F(\boldsymbol{k}, \omega) \, w(\boldsymbol{k}, \omega) , \qquad (60)$$

where $w = \boldsymbol{v} \cdot \hat{\boldsymbol{z}}$. The function F includes the instrumental optical transfer function (OTF), which is the Fourier transform of the point-spread function of the telescope optics, as well as the effect of the finite pixel size of the detector. We use an azimuthal average of the OTF estimated by Tarbell, Acton, & Frank (1997) for the MDI/SOHO telescope in its high-resolution mode near disk center. We correct the OTF for the effect of finite pixel size, ϵ, by multiplying by $\text{sinc}(k\epsilon/2)$, with $\epsilon = 0.83$ Mm and $k = \|\boldsymbol{k}\|$.

In general, F also includes the filter used to select the particular waves of interest in the k-ω diagram and to remove low-frequency noise from the data. In this example there is only one ridge in the k-ω diagram, corresponding to the surface gravity waves. We choose a filter that is zero for frequencies less than $\omega_{\min}/2\pi = 2$ mHz and more than $\omega_{\max}/2\pi = 4$ mHz, as was done for the data shown in Figure 1.

We include an additional factor, R, in the filter to make our unstratified example look more solar. The function $R(k)$ is the ratio of mode inertia in our model to mode inertia in a standard stratified solar model:

$$R(k) = \frac{\rho \int_{-\infty}^{0} e^{2kz} \, dz}{\int_{-\infty}^{z_*} \rho_{\odot}(z) e^{2kz} \, dz} . \qquad (61)$$

Here ρ is the constant density in our model, and $\rho_{\odot}$ is the density as a function of height in the solar model. We use the solar model of Christensen-Dalsgaard, Proffit, & Thompson (1993) complemented by the chromospheric model of Vernazza, Avrett, & Loeser (1981) up to $z_* = 2$ Mm. In the solar model $z = 0$ is the photosphere. If we had started from the full stratified solar problem we would presumably obtain a solar-like power spectrum without this correction factor.

To summarize, we take the filter F to be

$$F(\boldsymbol{k}, \omega) = \text{OTF}(k) \, R(k) \, \text{Hea}(\omega - \omega_{\min}) \, \text{Hea}(\omega_{\max} - \omega) , \qquad (62)$$
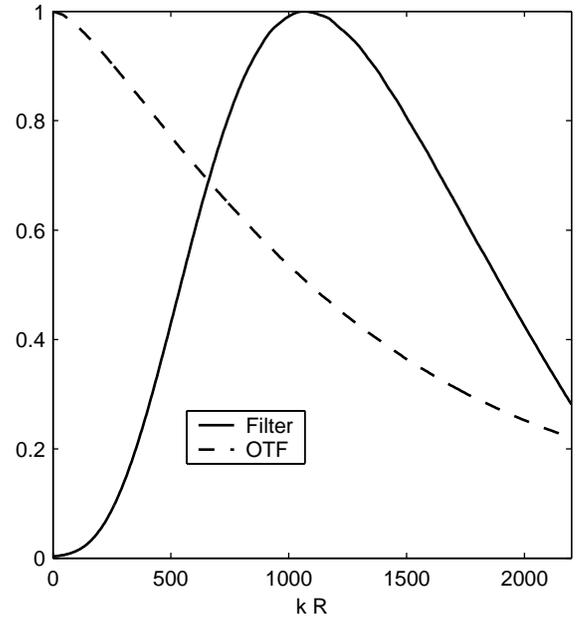
Fig. 5.—Wavenumber dependence of the filter F and of the OTF for the example calculation. Dashed line shows the azimuthal average of the OTF estimated by Tarbell et al. (1997) for the MDI/SOHO high-resolution telescope. The filter F is the product of the OTF and the mode-mass correction R given by eq. (61). Note that the mode-mass correction suppresses the low-wavenumber part of the spectrum, which gives better agreement between our unstratified model and a stratified solar model, for which low-wavenumber modes are difficult to excite.

where 'Hea' is the Heaviside step function. The OTF and the k-dependence of the full filter, F, are shown in Figure 5. We repeat that we have not included the effect of an observational time window, nor the effect of observing a finite area on the Sun. Both of these effects could be included, although the filter could no longer be represented as a simple multiplication in the Fourier domain.

3.2.5. Measurement of Travel Times

As explained in § 2.1, the observer needs to select the reference wavelet C^{ref} and the window function f in order to make a travel-time measurement. For this example, we choose C^{ref} to be the zero-order cross-correlation of the model,

$$C^{\text{ref}}(\boldsymbol{1}, \, \boldsymbol{2}, \, t) = C^0(\boldsymbol{1}, \, \boldsymbol{2}, \, t) , \qquad (63)$$

and the window function f to be the Heaviside step function,

$$f(t) = \text{Hea}(t) . \qquad (64)$$

For this choice of reference wavelet, the zero-order travel times $\tau_{\pm}^0$ are zero (see Appendix A). The window function f is acceptable, as we have only a single skip (surface waves). Using equation (A8), we rewrite the travel-time perturbations $\delta\tau_{\pm}$ in terms of the temporal Fourier transforms of $W_{\pm}$ and δC:

$$\delta\tau_{\pm}(\boldsymbol{1}, \, \boldsymbol{2}) = 4\pi \text{Re} \int_0^{\infty} d\omega \, W_{\pm}^*(\boldsymbol{1}, \, \boldsymbol{2}, \, \omega) \, \delta C(\boldsymbol{1}, \, \boldsymbol{2}, \, \omega) , \qquad (65)$$

where Re selects the real part of the expression. The real and

imaginary parts of $W_\pm(\omega)$ form a Hilbert transform pair:

$$W_\pm^*(\mathbf{1},\ \mathbf{2},\ \omega) = \frac{-\text{Hilb}[\omega C^0(\mathbf{1},\ \mathbf{2},\ \omega)] \mp i\omega C^0(\mathbf{1},\ \mathbf{2},\ \omega)}{4\pi \int_0^\infty \omega'^2 |C^0(\mathbf{1},\ \mathbf{2},\ \omega')|^2 d\omega'},$$

(66)

where Hilb[. . .] denotes the Hilbert transform (Saff & Snider 1993). Note that we used the fact that $C^0(t)$ is even, as will be shown in § 3.3.3. We now have an explicit definition of the travel-time perturbations $\delta\tau_+$ and $\delta\tau_-$ for our example.

The mean travel-time perturbation, $\delta\tau_{\text{mean}}$, and the travel-time difference, $\delta\tau_{\text{diff}}$, can be expressed in the form of equation (65) with weight functions $W_{\text{mean}}^*(\omega)$ and $W_{\text{diff}}^*(\omega)$, given by

$$W_{\text{mean}}^* = \tfrac{1}{2}\left(W_+^* + W_-^*\right), \quad (67)$$
$$W_{\text{diff}}^* = W_+^* - W_-^* . \quad (68)$$

From equation (66), and because $C^0(\omega)$ is real, we see that $W_{\text{mean}}^*(\omega)$ is real and that $W_{\text{diff}}^*(\omega)$ is imaginary. Thus the real part of the perturbation to the cross-correlation, $\delta C(\omega)$, introduces a mean travel-time perturbation. The imaginary part of $\delta C(\omega)$ causes a travel-time difference.

3.3. Zero-Order Solution

Now that the problem has been fully specified, we can compute the Green's function (§ 3.3.1), the power spectrum (§ 3.3.2), and the cross-correlation for the zero-order model (§ 3.3.3). We show that the power spectrum in our example resembles the solar f-mode spectrum. We find that the unperturbed cross-correlation is the inverse Fourier transform of the power spectrum.

3.3.1. Green's Function

Here we derive the Green's function appropriate for solving a problem of the form of equation (42). The vector Green's function, $\mathbf{G}(\mathbf{x},z,t;\mathbf{s},t_s)$, is the velocity response at horizontal coordinate $\mathbf{x}$, height z, and time t to an impulsive source in S at surface location $\mathbf{s}$ and time t_s. In our example S is scalar, so we need only one vector Green's function, and we drop the superscript on the Green's function, which appeared in the general theory (eq. [16]). By definition, $\mathbf{G}$ solves the surface boundary condition

$$\mathcal{L}^0 \mathbf{G}(\mathbf{x},z,t;\mathbf{s},t_s) = \delta_D(\mathbf{x}-\mathbf{s})\delta_D(t-t_s) \quad \text{at } z=0, \quad (69)$$

with the additional constraints that $\mathbf{G}$ must be irrotational and divergenceless in the bulk, as well as vanish as $z \to -\infty$. The Green's function $\mathbf{G}$ is only a function of the horizontal spatial separation $\mathbf{x}-\mathbf{s}$, the time lag $t-t_s$, and the observation height z. Using the Fourier convention given by equation (B4), the Fourier transform of the Green's function can be written

$$\mathbf{G}(\mathbf{k},\omega;z) = \frac{(i\hat{\mathbf{k}}+\hat{\mathbf{z}})e^{kz}}{(2\pi)^3 k[gk-\omega^2 - i\omega\Gamma^0(\omega)]}, \quad (70)$$

where $\hat{\mathbf{k}} = \mathbf{k}/k$. We remind the reader that in this example the wavevector $\mathbf{k}$ is horizontal. From the above expression we can see that the horizontal component of $\mathbf{G}(\mathbf{k},\omega;z)$ is in the direction of $\mathbf{k}$ and that the horizontal and vertical components are of the same magnitude and $\pi/2$ out of phase. The amplitude of the Green's function decays exponentially with depth; the same result would apply for a vertically

stratified medium (Lamb 1932). At fixed wavenumber k, the Green's function has resonant frequencies $\omega \simeq \pm(gk)^{1/2} - i\Gamma^0/2$ in the limit of small damping. We recognize the dispersion relation for deep water waves. Since $\Gamma^0(\omega)$ is positive, the imaginary part of the two poles of the Green's function is negative. This ensures that the Green's function is causal (e.g., Saff & Snider 1993). For later use, we also introduce another Green's function,

$$\mathscr{G}^\Pi(\mathbf{k},\omega) = i\omega k^2 F(\mathbf{k},\omega)G_z(\mathbf{k},\omega,z=0), \quad (71)$$

which gives the vertical velocity at the surface resulting from an impulsive source in Π/ρ. The Green's function G_z is the $\hat{\mathbf{z}}$ component of $\mathbf{G}$ given by equation (70).

3.3.2. Power

By definition, the power spectrum is the square of the modulus of the Fourier transform of the observable. For convenience, we consider the zero-order power spectrum per unit area and per unit time:

$$P(\mathbf{k},\omega) = \frac{(2\pi)^3}{AT} E\left[|\phi^0(\mathbf{k},\omega)|^2\right], \quad (72)$$

where A is the area and T the time interval over which the power is computed. After a few simple manipulations, we find that P is given by

$$P(\mathbf{k},\omega) = (2\pi)^6 |\mathscr{G}^\Pi(\mathbf{k},\omega)|^2 m^0(\mathbf{k},\omega). \quad (73)$$

None of the terms in the above equation depend on the direction of $\mathbf{k}$. In particular, $m^0 = m^0(k,\omega)$ because the sources are spatially homogeneous and isotropic in the zero-order problem. In addition, the filter F is a function only of the wavenumber k and frequency ω. Therefore, the power spectrum is independent of the direction of $\mathbf{k}$. The term $|\mathscr{G}^\Pi(\mathbf{k},\omega)|^2$ specifies the shape of the resonance peaks in the power spectrum. For ω near $(gk)^{1/2}$ we have approximately

$$P(\mathbf{k},\omega) \sim \frac{k^2 F^2 m^0}{4} \left[\left(\omega - \sqrt{gk}\right)^2 + \left(\frac{\Gamma^0}{2}\right)^2\right]^{-1}. \quad (74)$$

Thus, at fixed wavenumber, the line shape is Lorentzian, with full width at half-maximum $\Gamma^0(\omega)$.

Figure 6 compares the power spectrum for our model, $P(k,\omega)$, with the power spectrum for the solar f-mode ridge observed with the MDI/SOHO high-resolution telescope. The distribution of power with frequency and wavenumber confirms that there is a good agreement between the model and the observations.

3.3.3. Cross-Correlation

To obtain the zero-order cross-correlation, we use the definition of C^0 (eq. [22]), the expression for the source covariance (eq. [49]), and the definition of the Fourier transform to obtain

$$C^0(\mathbf{1},\ \mathbf{2},\ t) = \int\!\!\int_{-\infty}^\infty d\mathbf{k} \int_{-\infty}^\infty d\omega\, e^{i\mathbf{k}\cdot\Delta - i\omega t} P(\mathbf{k},\omega), \quad (75)$$

where $\Delta = \mathbf{2} - \mathbf{1}$. For the zero-order problem the cross-correlation is therefore the inverse Fourier transform of the power spectrum. This is a consequence of the fact that the problem is translation invariant. Since in our example P
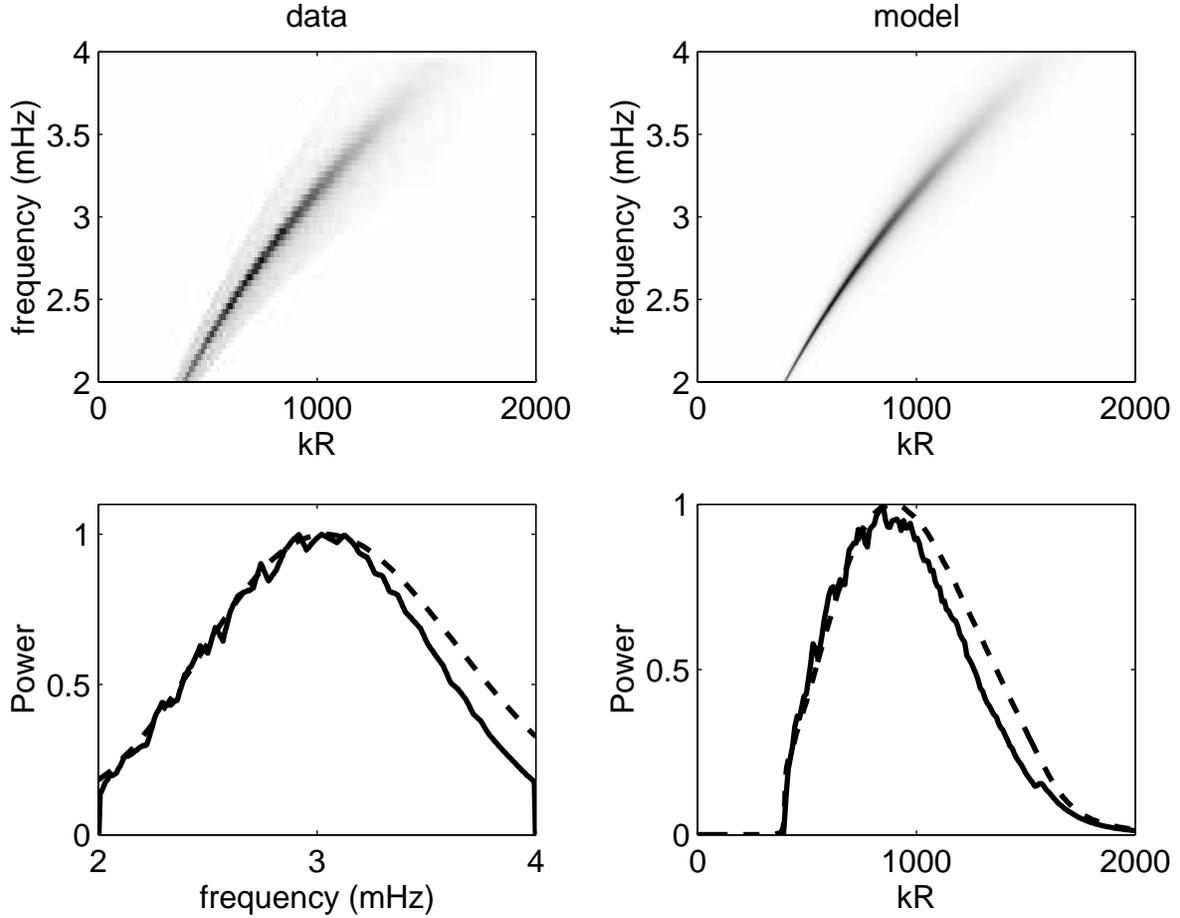
Fig. 6.—Comparison of observed and model power spectra. *Top right*: Zero-order power spectrum in our model, $P(k, \omega)$, defined by eq. (73). The coordinates are frequency, $\omega/2\pi$, and dimensionless wavenumber, $kR_\odot$, where $R_\odot = 696$ Mm is the solar radius. *Top left*: Azimuthal average of the power observed with the MDI/*SOHO* high-resolution telescope. The *f*-mode ridge has been isolated by a simple boxcar filter. *Bottom left*: Power integrated over wavenumber, as a function of frequency. The dashed and solid lines refer to the model and the observations, respectively. *Bottom right*: Power integrated over frequency, as a function of wavenumber $kR_\odot$. Again, the dotted line refers to the model and the solid line to the data. In our model the source correlation length and time are $L_s = 0$ and $T_s = 400$ s. The agreement between the model and the observations could be further improved by considering a nonzero source correlation length, which would reduce the power at high spatial frequencies.

does not depend on the direction of k, we can perform the integration over the angle between k and Δ to obtain

$$C^0(\mathbf{1}, \mathbf{2}, t) = 2\pi \int_0^\infty k\, dk \int_{-\infty}^\infty d\omega\, e^{-i\omega t} J_0(k\Delta) P(k, \omega) ,$$
$$(76)$$

where J_0 is the cylindrical Bessel function of order zero. From the above expression it is clear that the zero-order cross-correlation is only a function of the time lag t and the spatial separation between $\mathbf{1}$ and $\mathbf{2}$, $\Delta = \|\mathbf{\Delta}\|$. Note that the amplitude of the cross-correlation falls off as $\Delta^{-1/2}$ at large distances as a result of the asymptotic form of $J_0(k\Delta)$. This factor accounts for the geometrical spreading of two-dimensional waves, like surface-gravity waves.

From the power spectrum, we can compute numerically the cross-correlation using equation (76). Figure 1 provides a comparison between the model cross-correlation C^0 (*right panel*) and the average MDI cross-correlation for the *f*-mode (*left panel*). The two cross-correlations show the same features, including at very short distances. The two branches of the cross-correlation correspond to the propagation of the energy of the wave packets at the group speed,

$v_g = g/2\omega$, where ω is the central frequency. For a central frequency of 3 mHz the group speed is 7.3 km s^{-1}. The effect of dispersion is also clearly visible: the oscillating fine structure has a different slope from the envelope slope, given by the phase speed $v_p = 2v_g$. Low-frequency waves propagate faster than high-frequency waves, because the phase speed is inversely proportional to ω. Note that for distances less than about half a wavelength (2.5 Mm), the two branches of the cross-correlation are merged. This implies that travel-time measurements are difficult in the near field. The effect of damping is to strongly suppress high-frequency waves at large distances. Figure 2 shows a plot of the zero-order cross-correlation, $C^0 = C^{\text{ref}}$, at a distance $\Delta = 10$ Mm. As a consequence of the dependence of the phase speed on frequency (dispersion), the instantaneous frequency of the cross-correlation is seen to increase with time lag t.

3.4. *Kernels for Source Strength and Damping Rate*

In this section we derive travel-time kernels, $K_\pm^a$ and $K_\pm^\gamma$, for perturbations to the local source strength and damping rate, respectively. These kernels connect travel-time pertur-

bations $\delta\tau_\pm$ to fractional perturbations to the model,

$$\delta\tau_\pm(\mathbf{1},\ \mathbf{2}) = \int_{(A)} d\mathbf{r}\,\frac{\delta a(\mathbf{r})}{a}\,K_\pm^a(\mathbf{1},\ \mathbf{2};\mathbf{r})$$
$$+ \int_{(A)} d\mathbf{r}\,\frac{\delta\gamma(\mathbf{r})}{\gamma}\,K_\pm^\gamma(\mathbf{1},\ \mathbf{2};\mathbf{r})\ . \qquad (77)$$

Here $\delta a(\mathbf{r})/a$ is the local fractional change in the source strength and $\delta\gamma(\mathbf{r})/\gamma$ the fractional change in damping rate. The two-dimensional integrals are taken over all points $\mathbf{r}$ on the surface $z = 0$, denoted by (A).

In Appendix C we give an explicit derivation of the sensitivity kernels $K_\pm^\gamma$ and $K_\pm^a$. We first compute the sensitivity of the cross-correlation to small local changes in a and γ (eqs. [C2], [C3], and [C4]). We then relate changes in the cross-correlation to changes in travel times, through the weight functions $W_\pm$ (eq. [30]). Because of the assumptions that we have made in this example, the kernels can be written in terms of separate one-dimensional integrals over horizontal wavenumber. In Appendix C we show that $K_\pm^a$ are given by

$$K_\pm^a(\mathbf{1},\ \mathbf{2};\mathbf{r}) = 4\pi\,\mathrm{Re}\int_0^\infty d\omega\,W_\pm^*(\mathbf{1},\ \mathbf{2},\ \omega)m^0(\omega)$$
$$\times\,\mathrm{I}^*(\Delta_1,\omega)\mathrm{I}(\Delta_2,\omega)\ , \qquad (78)$$

where the integral $\mathrm{I}(d,\omega)$ is a function of a distance d and frequency ω only:

$$\mathrm{I}(d,\omega) = (2\pi)^3\int_0^\infty k\,dk\,J_0(kd)\mathscr{G}^\Pi(k,\omega)\ . \qquad (79)$$

In equation (78), Δ_1 is the distance from $\mathbf{1}$ to $\mathbf{r}$ and Δ_2 is the distance from $\mathbf{2}$ to $\mathbf{r}$. The complex integral $\mathrm{I}(d,\omega)/(2\pi)^2$ is the spatial inverse Fourier transform of the Green's function $\mathscr{G}^\Pi(\mathbf{k},\omega)$.

As shown in Appendix C, the damping kernels $K_\pm^\gamma$ can also be written as combinations of two one-dimensional integrals, $\mathrm{II}(d,\omega)$ and $\mathrm{III}(d,\omega)$:

$$K_\pm^\gamma(\mathbf{1},\ \mathbf{2};\mathbf{r}) = 4\pi(\hat{\mathbf{\Delta}}_1\cdot\hat{\mathbf{\Delta}}_2)\,\mathrm{Re}\int_0^\infty d\omega\,W_\pm^*(\mathbf{1},\ \mathbf{2},\ \omega)$$
$$\times\,m^0(\omega)\big[\mathrm{II}(\Delta_1,\omega)\mathrm{III}(\Delta_2,\omega)$$
$$+\,\mathrm{II}(\Delta_2,\omega)\mathrm{III}^*(\Delta_1,\omega)\big]\ , \qquad (80)$$

where $\hat{\mathbf{\Delta}}_1$ is a unit vector in the direction $\mathbf{r} - \mathbf{1}$ and $\hat{\mathbf{\Delta}}_2$ is a unit vector in the direction $\mathbf{r} - \mathbf{2}$. The explicit forms of II and III are given in Appendix C. The function III is complex and involves only one Green's function, $\mathscr{G}^\Pi$. The real integral II involves two Green's functions, G_z and $\mathscr{G}^\Pi$, and is related to the scattering process (see Fig. 3).

We computed the kernels numerically, with grid spacings of 7×10^{-3} rad Mm^{-1} in k and 10^{-2} mHz in $\omega/2\pi$, which were selected so that the smallest line widths (1.5×10^{-2} rad Mm^{-1}, 1.7×10^{-2} mHz) would be resolved. We ran a second set of calculations at twice the above stated resolutions and saw only very minor changes in the resulting kernels.

Figures 7a and 7b show the kernels $K_+^a(\mathbf{1},\ \mathbf{2};\mathbf{r})$ and $K_+^\gamma(\mathbf{1},\ \mathbf{2};\mathbf{r})$ for the distance $\Delta = 10$ Mm, as a functions of horizontal position $\mathbf{r} = (x,y)$. The observation points $\mathbf{1}$ and $\mathbf{2}$ have coordinates $(x_1,y_1) = (-5,\ 0)$ Mm and $(x_2,y_2) = (5,\ 0)$ Mm, respectively. An important observation is that the kernels K_+^a and K_+^γ are quite different: they do not simply have opposite signs. This means that a decrease in source strength is not equivalent to an increase

in damping rate, as one might naively expect. In particular, the total integral of the source kernel is zero, while the total integral of the damping kernel is positive, with a value of 5.9 s. A uniform increase in source strength results only in a change in the overall amplitude of the power spectrum (and thus in the cross-correlation) and as a result does not affect the travel time. In contrast, a uniform increase in the damping rate affects the shape of the power spectrum, and thus causes a travel-time perturbation $\delta\tau_+$. The kernels $K_+^{a,\gamma}$ have largest amplitude in the vicinity of the observation points $\mathbf{1}$ and $\mathbf{2}$. Both K_+^γ and K_+^a have roughly the same magnitude, of the order a few s Mm^{-2}. Both of the kernels oscillate spatially; this is a finite wavelength effect.

Hyperbola-shaped features (with $\Delta_2 - \Delta_1 = \mathrm{const}$) are present in both K_+^γ and K_+^a. As Woodard (1997) noted, all of the sources located along a particular hyperbola (with foci at the observation points) give a similar contribution to the cross-correlation, which explains the appearance of the kernel K_+^a. We emphasize that the kernel $K_+^a(\mathbf{1},\ \mathbf{2};\mathbf{r})$ is for the one-way travel time $\delta\tau_+(\mathbf{1},\ \mathbf{2})$, which relates to waves moving from $\mathbf{1}$ to $\mathbf{2}$. As a result, only perturbations to the sources that produce waves moving from $\mathbf{1}$ to $\mathbf{2}$ can introduce a perturbation in $\tau_+(\mathbf{1},\ \mathbf{2})$. This is clear from Figure 7a: the kernel K_+^a is only significant in the region $x < 0$, which produces waves that arrive at $\mathbf{1}$ before they arrive at $\mathbf{2}$.

The damping kernel K_+^γ is more complicated, as it shows ellipses ($\Delta_2 + \Delta_1 = \mathrm{const}$) in addition to hyperbolas, and results from scattering, unlike the source strength kernel. The ellipses are due to waves that go through $\mathbf{1}$, scatter at $\mathbf{r}$, and are then observed at $\mathbf{2}$. The hyperbolas corresponds to scattered waves that arrive at $\mathbf{1}$ before the direct waves arrive at $\mathbf{2}$. Note that the damping kernels K^γ change sign on the circle $\hat{\mathbf{\Delta}}_1\cdot\hat{\mathbf{\Delta}}_2 = 0$, which goes through $\mathbf{1}$ and $\mathbf{2}$. This is a result of the details of the scattering of waves by local inhomogeneities in the damping rate. The scattered wave depends on the direction of the incoming wave; back-scattered waves are in antiphase with forward-scattered waves.

In this example, because $C^{\mathrm{ref}} = C^0$ is even in time, $\delta\tau_-(\mathbf{1},\ \mathbf{2}) = \delta\tau_+(\mathbf{2},\ \mathbf{1})$. As a result the kernels K_-, for the travel-time perturbation $\delta\tau_-$, can be obtained from

$$K_-(\mathbf{1},\ \mathbf{2};\mathbf{r}) = K_+(\mathbf{2},\ \mathbf{1};\mathbf{r})\ . \qquad (81)$$

This is not, however, a general rule; it depends on the choice of reference wavelet. The kernels for the perturbations to the travel-time mean and difference can be easily obtained from the kernels for the one-way travel times:

$$K_{\mathrm{mean}}^{a,\gamma} = \tfrac{1}{2}\big(K_+^{a,\gamma} + K_-^{a,\gamma}\big)\ , \qquad (82)$$
$$K_{\mathrm{diff}}^{a,\gamma} = K_+^{a,\gamma} - K_-^{a,\gamma}\ . \qquad (83)$$

The kernels $K_{\mathrm{mean}}^{a,\gamma}$ and $K_{\mathrm{diff}}^{a,\gamma}$ are plotted in the remaining panels of Figure 7.

The kernels for the mean travel time are symmetric on interchange of $\mathbf{1}$ and $\mathbf{2}$, and the travel-time difference kernels are antisymmetric on interchange of $\mathbf{1}$ and $\mathbf{2}$. Note that like the one-way travel time kernels, the kernels $K_{\mathrm{diff}}^{a,\gamma}$ and $K_{\mathrm{mean}}^{a,\gamma}$ are largest near the observation points $\mathbf{1}$ and $\mathbf{2}$. We note that K_{diff}^a is roughly of the opposite sign to K_{diff}^γ, except inside the circle defined by $\hat{\mathbf{\Delta}}_1\cdot\hat{\mathbf{\Delta}}_2 = 0$, where the sign is the same. A localized perturbation to source strength (damping rate) on the line $y = 0$ with $x \lesssim x_1$ gives an increase (decrease) in the travel-time difference.
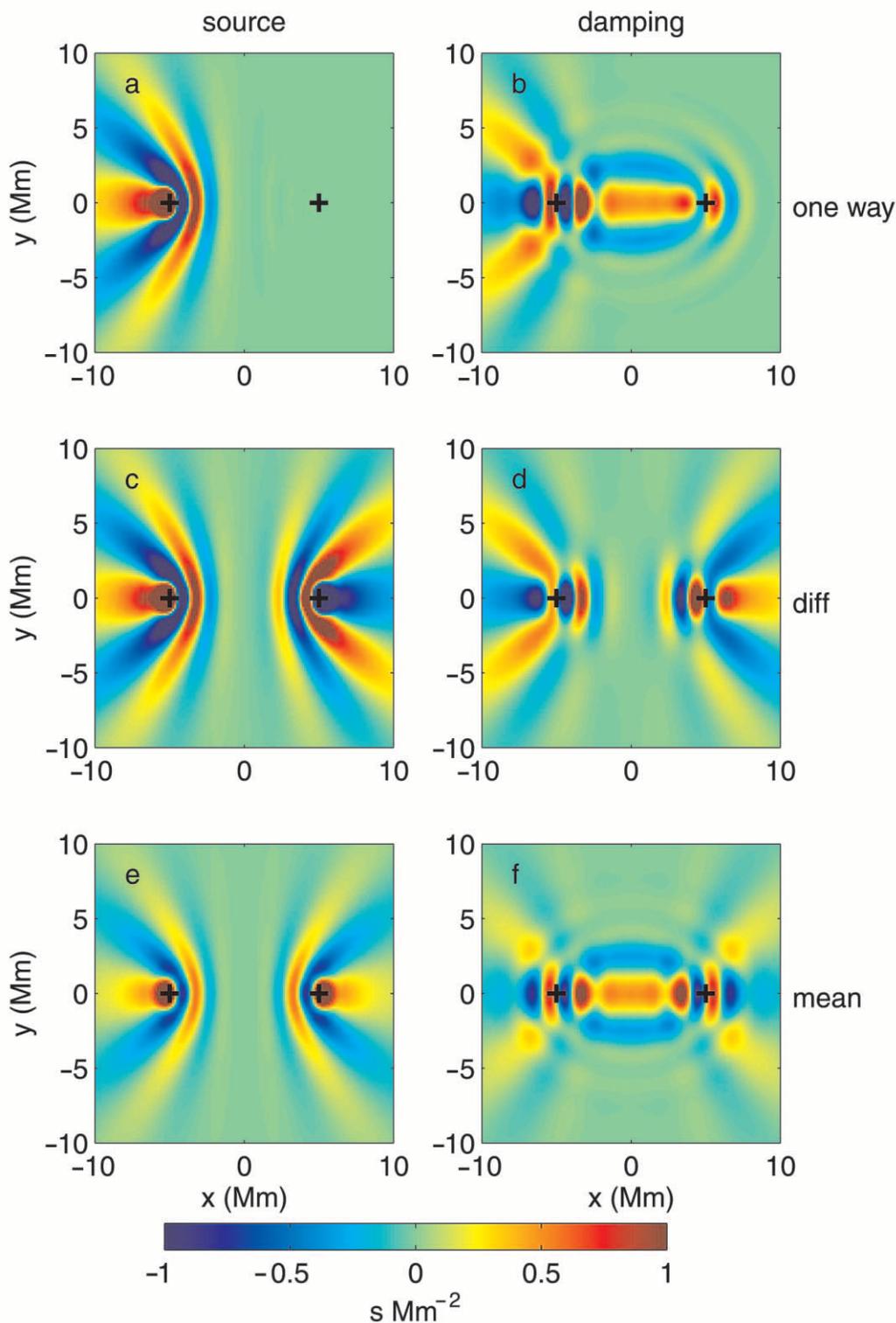
Fig. 7.—Travel-time sensitivity kernels for perturbations in source strength and damping rate as functions of position $\mathbf{r} = (x, y)$. The left column displays kernels for source strength, K^a, and the right column displays kernels for damping rate, K^γ. The top row gives the one-way travel-time kernels $K_+^{a,\gamma}$, the middle row gives the travel-time difference kernels $K_{\text{diff}}^{a,\gamma}$, and the bottom row gives the mean travel-time kernels $K_{\text{mean}}^{a,\gamma}$. The observation points 1 and 2 have the coordinates $(x_1, y_1) = (-5, 0)$ Mm and $(x_2, y_2) = (5, 0)$ Mm, respectively, and are denoted by the black crosses in each panel. The color scale indicates the local value of the kernel, with blue representing negative value and red positive. The color scale is truncated at ± 1 s Mm^{-2}. The grid spacing is 0.14 Mm.

In order to show the full range of variation of the kernels we plot, in Figure 8, cuts of the kernels $K_+^{a,\gamma}$ along the lines $y = 0$ and $x = 0$. Figure 8a shows that the source kernel is zero along the line $x = 0$, while the damping kernel is positive and maximum at $y = 0$. The side lobes (the second Fresnel zone) of K_+^γ extend out to 3.5 Mm. The slice along the line $y = 0$, Figure 8b, shows the complicated behavior of the kernels near the observation points, where they oscillate.

We have studied single-frequency kernels and seen that there is constructive interference between different fre-
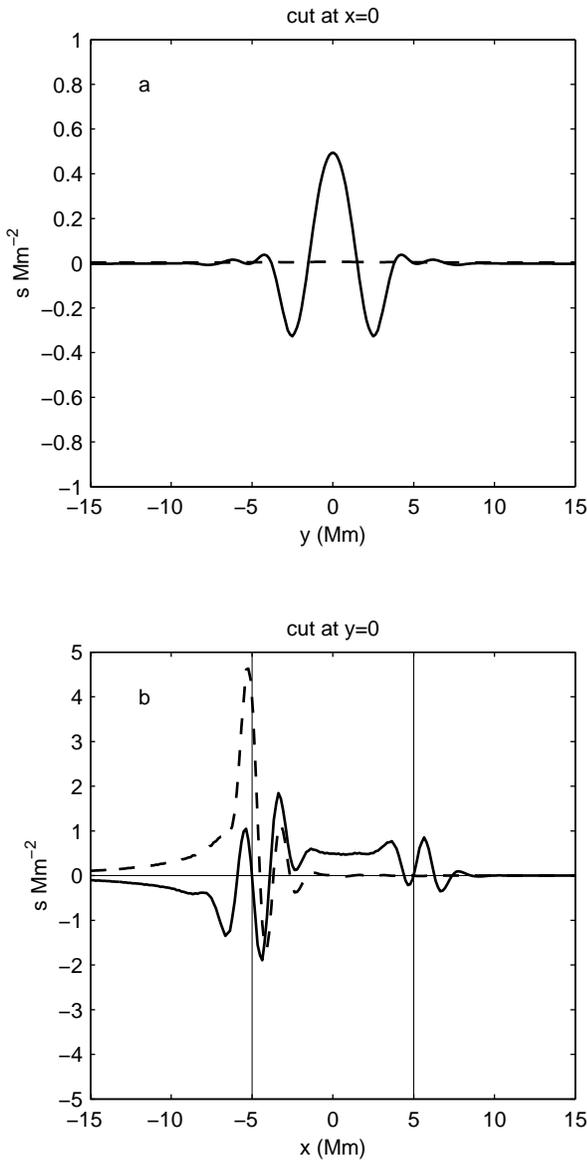
FIG. 8.—Cuts through the source and damping kernels, K_+^a and K_+^γ. Panel a shows cuts along the line $x = 0$, and panel b shows cuts along the line $y = 0$. The dashed line is for the source kernel K_+^a, and the solid line is for the damping kernel K_+^γ.

quency components along the line $y = 0$, $-\infty < x < x_2$ for K_+^γ, and the line $y = 0$, $-\infty < x < x_1$ for K_+^a. In the limit of infinite bandwidth, the kernels K_+^γ and K_+^a reduce to these rays, respectively. This is in contrast to conventional ray theory, in which the ray is restricted to the line segment $y = 0$, $x_1 < x < x_2$.

In the past, travel-time kernels have been calculated in the "single-source picture" (Birch & Kosovichev 2000; Jensen et al. 2000). In the following section we test the single-source method by comparing single-source kernels with the kernels calculated using a random distributed source model.

3.5. *The Single-Source Picture*

The single-source picture consists of placing a single causal source at **1** and observing the effect of local perturbations on the wave field observed at **2**. The one-way travel-

time perturbation is approximated by the travel-time shift,

$$\delta\tau_+^{ss}(\mathbf{1}, \mathbf{2}) = -\frac{\int_{-\infty}^\infty dt\, \delta\phi(\mathbf{2}, t)\, \dot{\phi}^0(\mathbf{2}, t)}{\int_{-\infty}^\infty dt\, [\dot{\phi}^0(\mathbf{2}, t)]^2}, \quad (84)$$

between the unperturbed and perturbed signals at **2** (Birch & Kosovichev 2001). This new definition of travel time is necessary: in the single-source picture there is no cross-correlation, and thus our earlier definition of travel time cannot be used. In equation (84), $\phi^0(\mathbf{2})$ and $\delta\phi(\mathbf{2})$ are the unperturbed and perturbed wave fields at **2**. The wave field is generated by a causal pressure source placed at **1**:

$$\Pi(\mathbf{s}, t_s) = \rho\, \Theta(\mathbf{s} - \mathbf{1}, t_s). \quad (85)$$

The function Θ characterizes the pressure source, and will later be used to tune the source spectrum.

In this section we consider the kernel $K_+^{\gamma,ss}$, derived in the single-source picture, which gives the sensitivity of the travel-time perturbation $\delta\tau_+$ to a local fractional perturbation in the damping rate. The single-source picture cannot easily be used to derive a kernel for a source perturbation, which does not involve a scattering process.

By definition, the kernel $K_+^{\gamma,ss}$, which we derive in Appendix D, satisfies

$$\delta\tau_+^{ss}(\mathbf{1}, \mathbf{2}) = \int_{(A)} d\mathbf{r}\, \frac{\delta\gamma(\mathbf{r})}{\gamma} K_+^{\gamma,ss}(\mathbf{1}, \mathbf{2}; \mathbf{r}). \quad (86)$$

The definition of travel time given in equation (84) closely resembles the definition of travel time used in the general theory (eqs. [A6] and [A8]) if $\phi(\mathbf{2}, t)$ looks like the positive time-lag branch of the zero-order cross-correlation from the random source model (§ 3.3.3). This condition implies that the spectrum of the source, $\Theta(\mathbf{k}, \omega)$, is given by equation (D8).

Figure 9 is a comparison of the single-source kernel $K_+^{\gamma,ss}$ with the distributed-source kernel K_+^γ, computed in § 3.4. The single-source kernel fails to reproduce the hyperbola-shaped features that are seen in the random source kernel, even though the ellipses can be seen in both (with the same order of magnitude and sign). A single causal source at **1** is not sufficient to generate all of the waves that are relevant to the problem of computing travel-time kernels (see Fig. 10).

Cuts at $y = 0$ through $K_+^{\gamma,ss}$ and K_+^γ are shown in Figure 11, again for the distance $\Delta = 10$ Mm that was used in all previous plots of kernels. The kernels agree well for $x \gtrsim 0$, where the hyperbola-shaped features in K_+^γ are absent. For $x \lesssim 0$, the two kernels are quite different; in particular, the single-source kernel is nearly zero for $x < -7$ Mm, while K_+^γ has a negative tail there.

In the limit of infinite bandwidth (ray theory), the single-source kernel $K_+^{\gamma,ss}$ would be restricted to the line segment, $y = 0$, $x_1 < x < x_2$, in contrast to the finding (see § 3.4) that the distributed-source kernel K_+^γ would reduce to the ray $y = 0$, $-\infty < x < x_2$.

4. DISCUSSION

We now have a general recipe (§ 2) for solving the linear forward problem, i.e., computing travel-time sensitivity kernels. This recipe is based on a physical description of the observed wave field. The kernels give the linear dependence of travel-time perturbations on perturbations
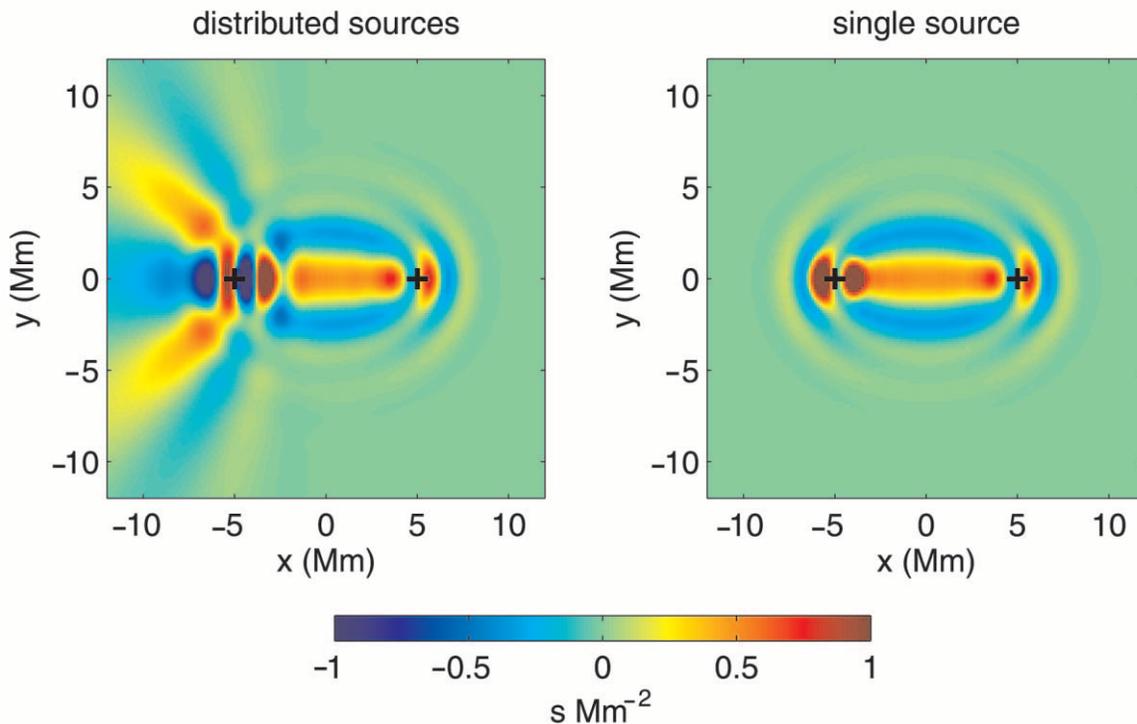
Fig. 9.—Comparison between single and distributed source kernels for damping rate. *Left*: distributed source kernel for damping, K_+^γ (also shown in Fig. 7b). *Right*: Single-source kernel $K_+^{\gamma,\mathrm{ss}}$ discussed in § 3.5 and computed using eqs. (D5) and (D6). For the single-source kernel the source is located at **1**, with coordinates $(-5, 0)$ Mm. The observation point **2** is located at $(0, 5)$ Mm.

to a solar model, and they take into account the details of the measurement procedure. The sensitivity kernels depend on the background solar model, the filtering and fitting of the data, and the position on the solar disk (through the line of sight).

In § 3 we have shown how to compute the two-dimensional sensitivity of travel-time perturbations to source and damping inhomogeneities for surface gravity waves. This example is important, as it shows that kernels can be obtained, using our recipe, once the physics of the model is
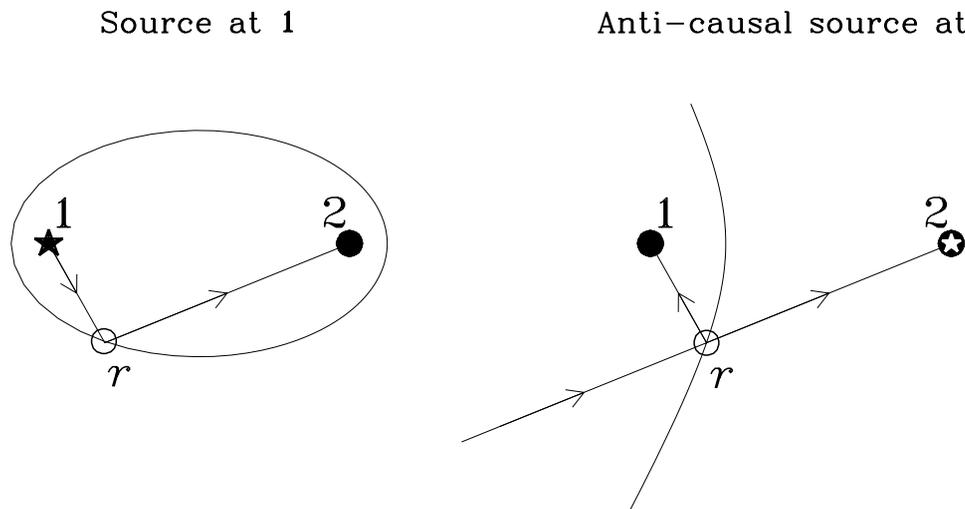
Fig. 10.—Graphical discussion of the single-source picture for computing kernels for the one-way travel time $\delta\tau_+(\mathbf{1}, \mathbf{2})$. The left panel is the conventional single-source picture, in which a causal source is exploded at **1** and the scattered wave is observed at **2**. The scattering point is denoted by $\mathbf{r}$. Perturbations located on curves with constant $\|\mathbf{r} - \mathbf{1}\| + \|\mathbf{2} - \mathbf{r}\|$ contribute to the scattered field with the same geometrical delay in travel time, and as a result ellipse-shaped features are seen in the travel-time kernel. A single source at **1** does not, however, produce all of the waves that are relevant to computing correct travel-time kernels. The right panel shows an example of a component to the wave field that is missed in the single-source picture. An anticausal source at **2** causes an incoming wave toward **2**, which is then scattered at $\mathbf{r}$ and arrives at **1**. For $\mathbf{r}$ near **1**, this gives a signal that is first observed at **1** and then later at **2**, i.e., looks like a wave moving from **1** to **2**. Perturbations located on curves with constant $\|\mathbf{r} - \mathbf{1}\| - \|\mathbf{2} - \mathbf{r}\|$, i.e., hyperbolas, contribute to the scattered field with the same geometrical delay in travel time (Woodward 1992). Were the single-source picture extended to include an anticausal source at **2**, hyperbola-shaped features would be seen in the travel-time kernels. Note, however, that hyperbolas naturally appear in the distributed-source kernels $K_+^{a,\gamma}$ (Figs. 7a and 7b). The hyperbolas with $\|\mathbf{r} - \mathbf{1}\| - \|\mathbf{2} - \mathbf{r}\| > 0$ are not seen, as they do not affect the positive-time branch of the cross-correlation (the scattered wave arrives at **1** after the unperturbed wave arrives at **2**).
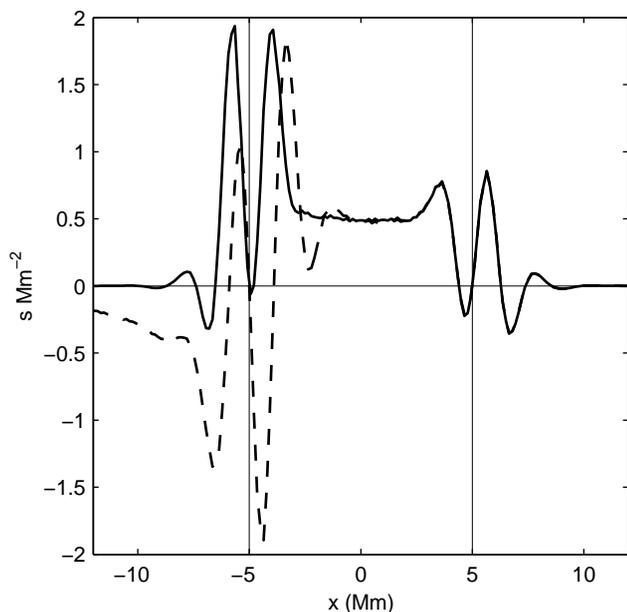
FIG. 11.—Cuts along the line $y = 0$ through the damping kernels K_+^γ and $K_+^{\gamma,ss}$ shown in Fig. 9. The dashed line is for the distributed-source kernel, and the solid line is for the single-source kernel.

fully specified. In particular, the source spectrum and the details of the observation procedure need to be specified at the start of the problem and appear explicitly in the expression for the travel-time kernels.

The model with random-excitation sources reveals some important details in the sensitivity kernels that are not accounted for in the single-source model. In particular, the single-source kernels show only ellipse-shaped features, while the distributed-source kernels show both hyperbola- and ellipse-shaped features. Computations of kernels in the single-source picture are as difficult, both analytically and numerically, as for kernels in the distributed-source picture.

The example we have presented is a simplified model for the solar f-mode. Improvements to the model would include stratification, spherical geometry, compressibility, and a physical model of excitation and damping. In particular, in a compressible medium the effect of the conversion of p-modes into f-modes by scattering could be computed. Despite these limitations, we believe that our two-dimensional example kernels can be useful in studying solar problems using time-distance helioseismology. The kernels can be interpreted as depth averages over the first few Mm below the photosphere of the three-dimensional solar kernels (Duvall & Gizon 2000).

Woodard (1997) performed an analysis of the effect of localized damping on travel times for acoustic waves; this analysis showed that for a model sunspot, with radius 10 Mm, the travel-time difference is of the order of -1 minute, in the case where **1** is located at the center of the sunspot and **2** is a distance 10 Mm away. For the same geometry, the kernel K_{diff}^γ, which we have computed, predicts a positive travel-time difference of 1 s for a 50% increase in damping rate. These two apparently conflicting results are, however, for different types of waves and quite different models for the effect of damping inhomogeneities. The damping perturbation employed by Woodard (1997) can be understood in

terms of a reduction in source strength for sources located behind the sunspot from the observation points, as scattering by the damping inhomogeneities was neglected. Work remains to be done on this subject. For example, it is known that absorption by magnetic structures is a strong function of frequency (Braun, Duvall, & LaBonte 1988; Bogdan et al. 1993). This effect could be modeled by writing kernels for local changes to the exponent β in equation (57) for the damping rate. We plan to do a quantitative analysis of this problem in the future. Note that perturbations in sunspots are strong and that linear theory may not be accurate in this case (e.g., Cally & Bogdan 1997)

The most significant obstacle to the computation of accurate travel-time kernels is our lack of a detailed understanding of turbulent convection. The excitation and damping of solar oscillations is due to convection and is thus extremely difficult to account for in the background model; approximations must be introduced. For this paper we employed a phenomenological model based on observed properties of solar convection. An important constraint on the zero-order solar model is that it must produce a k-ω diagram compatible with observations. A further complication introduced by turbulence is that, in principle, it demands a theory for wave propagation through random media, i.e., a treatment of perturbations that vary on short temporal and spatial scales.

We have not addressed the computation of three-dimensional travel-time kernels in a spherical solar model. Preliminary efforts have shown that such a computation is feasible, but demanding (Birch & Kosovichev 2000).

There are a number of less fundamental issues relating to the interpretation of travel times. We emphasize that the filter $\mathscr{F}$ includes the point-spread function of the instrument, which is not always well known. It is unclear how an inaccurate estimate of the point-spread function affects the interpretation of travel-time measurements. A straightforward issue is that cross-correlations are typically averaged over annuli or sectors of annuli (Duvall et al. 1997); this can easily be accounted for by averaging the point-to-point kernels described in this paper.

The inverse problem, using measured travel times to learn about how the Sun differs from a model, is an entirely separate issue and beyond the scope of this paper. We wish to note, however, that techniques for the three-dimensional inversion of time-distance data have already been developed (Kosovichev 1996; Jensen et al. 1998). The errors in the travel-time measurements, which are essential to solving the inverse problem, are mainly due to realization noise. The formalism presented in this paper will be helpful in estimating these errors.

Despite all of the aforementioned difficulties, the approach we have described here is feasible, as we have seen in the example section. Gizon et al. (2000) have shown the same procedure to work with real f-mode data.

APPENDIX A

DEFINITION OF TRAVEL TIME

According to equation (5) the travel times $\tau_+(\mathbf{1},\ \mathbf{2})$ and $\tau_-(\mathbf{1},\ \mathbf{2})$ are the time lags that minimize the functions

$$X_\pm(\mathbf{1},\ \mathbf{2}, t) = \int_{-\infty}^{\infty} dt'\, f(\pm t') \left[C(\mathbf{1},\ \mathbf{2}, t') - C^{\mathrm{ref}}(\mathbf{1},\ \mathbf{2}, t' \mp t) \right]^2 . \tag{A1}$$

As a result, the time derivatives of $X_\pm$ evaluated at $\tau_\pm$ are zero:

$$\dot{X}_\pm(\mathbf{1},\ \mathbf{2}, \tau_\pm) = 0 . \tag{A2}$$

Note that $\dot{X}$ does not involve a time derivative of the observed cross-correlation C. In order to obtain the travel-time perturbations $\delta\tau_\pm$, we need to linearize around the zero-order travel times $\tau_\pm^0$, which are defined by

$$\tau_\pm^0(\mathbf{1},\ \mathbf{2}) = \arg\min_t \{ X_\pm^0(\mathbf{1},\ \mathbf{2}, t) \} . \tag{A3}$$

The functions $X_\pm^0$ refer to equation (A1) evaluated for $C = C^0$, where C^0 is the zero-order cross-correlation in the reference model. Linearizing equation (A2) about $\tau_\pm = \tau_\pm^0$ gives

$$\delta\tau_\pm(\mathbf{1},\ \mathbf{2}) = -\frac{\delta\dot{X}_\pm(\mathbf{1},\ \mathbf{2}, \tau_\pm^0)}{\ddot{X}_\pm^0(\mathbf{1},\ \mathbf{2}, \tau_\pm^0)} . \tag{A4}$$

The functions $\delta\dot{X}_\pm$ are given by

$$\delta\dot{X}_\pm(\mathbf{1},\ \mathbf{2}, t) = \pm 2 \int_{-\infty}^{\infty} dt'\, f(\pm t') \dot{C}^{\mathrm{ref}}(\mathbf{1},\ \mathbf{2}, t' \mp t)\, \delta C(\mathbf{1},\ \mathbf{2}, t') . \tag{A5}$$

We can then compute $\ddot{X}^0(\tau_\pm^0)$ by straightforward differentiation of equation (A1). The result for $\delta\tau_\pm(\mathbf{1},\ \mathbf{2})$ is thus

$$\delta\tau_\pm(\mathbf{1},\ \mathbf{2}) = \int_{-\infty}^{\infty} dt\, W_\pm(\mathbf{1},\ \mathbf{2}, t)\, \delta C(\mathbf{1},\ \mathbf{2}, t) , \tag{A6}$$

with

$$W_\pm(t) = \frac{\pm f(\pm t) \dot{C}^{\mathrm{ref}}(t \mp \tau_\pm^0)}{\int_{-\infty}^{\infty} dt' \left[f(\pm t') C^0(t') \ddot{C}^{\mathrm{ref}}(t' \mp \tau_\pm^0) \pm \dot{f}(\pm t') C^{\mathrm{ref}}(t' \mp \tau_\pm^0) \dot{C}^{\mathrm{ref}}(t' \mp \tau_\pm^0) \right]} . \tag{A7}$$

We have suppressed the spatial arguments $\mathbf{1}$ and $\mathbf{2}$ in the above equation for the sake of readability. This is the general linearized result for arbitrary C^{ref} and f. The only assumption is that the perturbation to the cross-correlation is small compared to the zero-order cross-correlation. Note that we have not written an explicit expression for $\tau_\pm^0$, which needs to be computed numerically by minimizing $X_\pm^0(t)$ (eq. [A3]).

In the case where C^{ref} and C^0 are even in time, $\tau_+^0 = \tau_-^0$. For the choice $C^{\mathrm{ref}} = C^0$, the zero-order travel times are both zero, $\tau_\pm^0 = 0$. This choice is recommended if a theoretical model is available to the observer. With $C^{\mathrm{ref}} = C^0$, the weight functions $W_\pm$ simplify to

$$W_\pm(\mathbf{1},\ \mathbf{2}, t) = \frac{\mp f(\pm t) \dot{C}^0(\mathbf{1},\ \mathbf{2}, t)}{\int_{-\infty}^{\infty} dt'\, f(\pm t') [\dot{C}^0(\mathbf{1},\ \mathbf{2}, t')]^2} . \tag{A8}$$

In the example presented in § 3, we choose $C^{\mathrm{ref}} = C^0$ and $f(t) = \mathrm{Hea}(t)$.

APPENDIX B

FOURIER CONVENTION FOR THE EXAMPLE SECTION

Given a function $q(\mathbf{x}, t)$, of horizontal position $\mathbf{x}$ and time t, we employ the convention that the function $q(\mathbf{x}, t)$ and its Fourier transform $\breve{q}(\mathbf{k}, \omega)$ are related by

$$q(\mathbf{x}, t) = \iint_{-\infty}^{\infty} d\mathbf{k} \int_{-\infty}^{\infty} d\omega\, e^{i\mathbf{k}\cdot\mathbf{x} - i\omega t} \breve{q}(\mathbf{k}, \omega) , \tag{B1}$$

$$\breve{q}(\mathbf{k}, \omega) = \frac{1}{(2\pi)^3} \iint_{-\infty}^{\infty} d\mathbf{x} \int_{-\infty}^{\infty} dt\, e^{-i\mathbf{k}\cdot\mathbf{x} + i\omega t} q(\mathbf{x}, t) , \tag{B2}$$

where $\mathbf{k}$ is a two-dimensional horizontal wavevector and ω is the angular frequency. We commonly use the same symbol for q and $\breve{q}$: the arguments make clear whether the function or its transform is intended. We use the notation $q(k, \omega)$ when $q(\mathbf{k}, \omega)$ only depends on the magnitude of $\mathbf{k}$, not its direction, for example in the filter function $F(k, \omega)$. We note that for functions

$q(\boldsymbol{x}, t)$ that do not vanish at large $\|\boldsymbol{x}\|$ or $|t|$ the Fourier transform is not defined. In particular, there is a problem for the case when the observable is not windowed in space or time. In such a case, $q(\boldsymbol{k}, \omega)$ is intended to mean the Fourier transform of the function $q(\boldsymbol{x}, t)$ truncated to zero for $|t| > T/2$ and $\|\boldsymbol{x}\| > (A/\pi)^{1/2}$, where the time interval T and the area A are both large and finite. This modification enables us to refer to the Fourier transform of a stationary/homogeneous random function (cf. Yaglom 1962, for a rigorous formalism).

When a function of four arguments, $Q(\boldsymbol{x}, t; \boldsymbol{x}', t')$, depends only on the separations $\boldsymbol{x} - \boldsymbol{x}'$ and $t - t'$ (translation invariance), we use the conventions

$$Q(\boldsymbol{x} - \boldsymbol{x}', t - t') = Q(\boldsymbol{x}, t; \boldsymbol{x}', t') , \tag{B3}$$

$$Q(\boldsymbol{k}, \omega) = \frac{1}{(2\pi)^3} \iint_{-\infty}^{\infty} d\boldsymbol{x} \int_{-\infty}^{\infty} dt \, e^{-i\boldsymbol{k}\cdot\boldsymbol{x}+i\omega t} Q(\boldsymbol{x}, t) . \tag{B4}$$

The above conventions are employed, in our example, for the functions $m^0(k, \omega)$, $\boldsymbol{G}(\boldsymbol{k}, \omega; z)$, and $\mathscr{G}(k, \omega)$.

Finally, we recall the relations

$$\int_{-\infty}^{\infty} dt \, e^{i\omega t} = 2\pi \, \delta_{\mathrm{D}}(\omega) , \tag{B5}$$

$$\iint_{-\infty}^{\infty} d\boldsymbol{x} \, e^{-i\boldsymbol{k}\cdot\boldsymbol{x}} = (2\pi)^2 \, \delta_{\mathrm{D}}(\boldsymbol{k}) , \tag{B6}$$

which are very useful in rewriting the kernels in Fourier space (Appendix C).

APPENDIX C

TRAVEL-TIME SENSITIVITY KERNELS FOR THE EXAMPLE

In this Appendix we derive surface gravity wave travel-time kernels, $K_\pm^a$ and $K_\pm^\gamma$, for perturbations to local source strength and damping rate, respectively. These kernels connect travel-time perturbations, $\delta\tau_\pm$, to perturbations to the model,

$$\delta\tau_\pm(\boldsymbol{1}, \, \boldsymbol{2}) = \int_{(A)} d\boldsymbol{r} \, \frac{\delta a(\boldsymbol{r})}{a} K_\pm^a(\boldsymbol{1}, \, \boldsymbol{2}; \boldsymbol{r}) + \int_{(A)} d\boldsymbol{r} \, \frac{\delta\gamma(\boldsymbol{r})}{\gamma} K_\pm^\gamma(\boldsymbol{1}, \, \boldsymbol{2}; \boldsymbol{r}) . \tag{C1}$$

Here $\delta a(\boldsymbol{r})/a$ is the local fractional change in the source strength, and $\delta\gamma(\boldsymbol{r})/\gamma$ is the local fractional change in damping rate. The spatial integral $\int_{(A)} d\boldsymbol{r}$ is a two-dimensional integral taken over all points $\boldsymbol{r}$ on the surface $z = 0$. From the theory part of this paper (§ 2), we know that in order to compute kernels we first need to write the perturbation to the cross-correlation in terms of the functions $\mathscr{C}^a$ and $\mathscr{C}^\gamma$ (see eq. [29]):

$$\delta C(\boldsymbol{1}, \, \boldsymbol{2}, t) = \int_{(A)} d\boldsymbol{r} \, \frac{\delta a(\boldsymbol{r})}{a} \mathscr{C}^a(\boldsymbol{1}, \, \boldsymbol{2}, t; \boldsymbol{r}) + \int_{(A)} d\boldsymbol{r} \, \frac{\delta\gamma(\boldsymbol{r})}{\gamma} \mathscr{C}^\gamma(\boldsymbol{1}, \, \boldsymbol{2}, t; \boldsymbol{r}) . \tag{C2}$$

The general expression for $\delta C(\boldsymbol{1}, \, \boldsymbol{2}, t)$ is given by equations (25), (26), and (27). In our example, however, the superscripts on the Green's function can be dropped, as the source S is scalar. To obtain $\mathscr{C}^a$, we use equation (27) for $\mathscr{C}_S$ and the definition of the source perturbation δM (eqs. [49] and [53]). After integrations by parts on the source variables in the right-hand side of equation (27) and the change of variables $\boldsymbol{r} = (\boldsymbol{s} + \boldsymbol{s}')/2$ and $\boldsymbol{u} = \boldsymbol{s} - \boldsymbol{s}'$, we obtain

$$\mathscr{C}^a(\boldsymbol{1}, \, \boldsymbol{2}, t; \boldsymbol{r}) = \frac{1}{T} \int dt' \, dt_s \, dt'_s \, d\boldsymbol{u} \, m^0(\boldsymbol{u}, t_s - t'_s) \mathscr{G}^{\Pi}\left(\boldsymbol{1} - \boldsymbol{r} - \frac{\boldsymbol{u}}{2}, t' - t_s\right) \mathscr{G}^{\Pi}\left(\boldsymbol{2} - \boldsymbol{r} + \frac{\boldsymbol{u}}{2}, t' - t'_s + t\right) . \tag{C3}$$

The function $\mathscr{C}^\gamma$ is obtained from equation (26) with $\delta\mathscr{L}$ defined by equations (46) and (58). After integrations by parts on the source variables, and a partial integration on the variable $\boldsymbol{r}$, the result is

$$\mathscr{C}^\gamma(\boldsymbol{1}, \, \boldsymbol{2}, t; \boldsymbol{r}) = \frac{1}{2\pi T} \int dt' \, dt'' \, d\boldsymbol{s} \, dt_s \, d\boldsymbol{s}' \, dt'_s \, d\bar{t} \, \Gamma^0(t'' - \bar{t}) m^0(\boldsymbol{s} - \boldsymbol{s}', t_s - t'_s) \nabla_h^2 \dot{\boldsymbol{G}}_h(\boldsymbol{r} - \boldsymbol{s}, \bar{t} - t_s)$$

$$\cdot \left[\mathscr{G}^{\Pi}(\boldsymbol{1} - \boldsymbol{s}', t' - t'_s) \nabla_h \dot{\mathscr{G}}(\boldsymbol{2} - \boldsymbol{r}, t' + t - t'') + \mathscr{G}^{\Pi}(\boldsymbol{2} - \boldsymbol{s}', t' + t - t'_s) \nabla_h \dot{\mathscr{G}}(\boldsymbol{1} - \boldsymbol{r}, t' - t'')\right] , \tag{C4}$$

where $\boldsymbol{G}_h$ denotes the two horizontal components of the vector $\boldsymbol{G}$. In the space-time domain these integrals are quite complicated to compute. They are, however, greatly simplified when written in terms of the Fourier transforms of the various functions:

$$\mathscr{C}^a(\boldsymbol{1}, \boldsymbol{2}, t; \boldsymbol{r}) = (2\pi)^4 \int d\omega \, d\boldsymbol{k} \, d\boldsymbol{k}' \, e^{i\boldsymbol{k}\cdot\boldsymbol{\Delta}_1 - i\boldsymbol{k}'\cdot\boldsymbol{\Delta}_2 - i\omega t} m^{0*}[(\boldsymbol{k} + \boldsymbol{k}')/2, \omega] \mathscr{G}^{\Pi*}(\boldsymbol{k}, \omega) \mathscr{G}^{\Pi}(\boldsymbol{k}', \omega) , \tag{C5}$$

$$\mathscr{C}^\gamma(\boldsymbol{1}, \boldsymbol{2}, t; \boldsymbol{r}) = (2\pi)^7 \int d\omega \, d\boldsymbol{k} \, d\boldsymbol{k}' \left(e^{i\boldsymbol{k}\cdot\boldsymbol{\Delta}_1 - i\boldsymbol{k}'\cdot\boldsymbol{\Delta}_2 - i\omega t} + e^{i\boldsymbol{k}\cdot\boldsymbol{\Delta}_2 - i\boldsymbol{k}'\cdot\boldsymbol{\Delta}_1 + i\omega t}\right)$$

$$\times \Gamma^0(\omega) m^0(\boldsymbol{k}, \omega) G^{\Pi}(\boldsymbol{k}, \omega) \mathscr{G}^{\Pi*}(\boldsymbol{k}, \omega) \hat{\boldsymbol{k}} \cdot \hat{\boldsymbol{k}}' \mathscr{G}^{\Pi}(\boldsymbol{k}', \omega)/k' . \tag{C6}$$

We have used the definitions

$$\mathscr{G}^{\Pi}(\boldsymbol{k}, \omega) = F(\boldsymbol{k}, \omega) G^{\Pi}(\boldsymbol{k}, \omega) , \tag{C7}$$

$$G^{\Pi}(\boldsymbol{k}, \omega) = i\omega k^2 G_z(\boldsymbol{k}, \omega; z = 0) , \tag{C8}$$

and the identity $\boldsymbol{G}_h(\boldsymbol{k}, \omega) = i\hat{\boldsymbol{k}} G_z(\boldsymbol{k}, \omega)$ resulting from equation (70). The Green's function $G_z(k, \omega)$ is the $\hat{\boldsymbol{z}}$ component of $\boldsymbol{G}$, given by equation (70).

With the assumption that m^0 is independent of $\boldsymbol{k}$, the above expressions can be simplified to

$$\mathscr{C}^a(\boldsymbol{1}, \ \boldsymbol{2}, \omega; \boldsymbol{r}) = m^0(\omega) \mathrm{I}^*(\Delta_1, \omega) \mathrm{I}(\Delta_2, \omega) , \tag{C9}$$

$$\mathscr{C}^\gamma(\boldsymbol{1}, \ \boldsymbol{2}, \omega; \boldsymbol{r}) = m^0(\omega) \hat{\boldsymbol{\Delta}}_1 \cdot \hat{\boldsymbol{\Delta}}_2 \big[\mathrm{II}(\Delta_1, \omega) \mathrm{III}(\Delta_2, \omega) + \mathrm{II}(\Delta_2, \omega) \mathrm{III}^*(\Delta_1, \omega) \big] . \tag{C10}$$

The integrals I, II, and III are given by

$$\mathrm{I}(d, \omega) = (2\pi)^3 \int_0^\infty k \, dk \, J_0(kd) \mathscr{G}^{\Pi}(k, \omega) , \tag{C11}$$

$$\mathrm{II}(d, \omega) = (2\pi)^6 \Gamma^0(\omega) \int_0^\infty k \, dk \, J_1(kd) G^{\Pi}(k, \omega) \mathscr{G}^{\Pi *}(k, \omega) , \tag{C12}$$

$$\mathrm{III}(d, \omega) = (2\pi)^3 \int_0^\infty dk \, J_1(kd) \mathscr{G}^{\Pi}(k, \omega) . \tag{C13}$$

The kernels for source strength and damping are then obtained from

$$K_\pm^{a,\gamma}(\boldsymbol{1}, \ \boldsymbol{2}, \boldsymbol{r}) = 4\pi \, \mathrm{Re} \int_0^\infty d\omega \, W_\pm^*(\boldsymbol{1}, \ \boldsymbol{2}, \omega) \mathscr{C}^{a,\gamma}(\boldsymbol{1}, \ \boldsymbol{2}, \omega; \boldsymbol{r}) , \tag{C14}$$

with $W_\pm^*(\boldsymbol{1}, \ \boldsymbol{2}, \omega)$ given by equation (66). The kernels, in terms of the integrals I, II, and III, are reported in the main body of the text (eqs. [78] and [80]).

APPENDIX D

SINGLE-SOURCE KERNELS FOR THE DAMPING RATE

In the single-source picture, we seek an expression for the kernel $K_+^{\gamma,\mathrm{ss}}$ that provides an integral relationship between the one-way travel time $\delta\tau_+^{\mathrm{ss}}$ (eq. [84]) and the local damping perturbation $\delta\gamma(\boldsymbol{r})/\gamma$, i.e.,

$$\delta\tau_+^{\mathrm{ss}}(\boldsymbol{1}, \ \boldsymbol{2}) = \int_{(A)} d\boldsymbol{r} \, \frac{\delta\gamma(\boldsymbol{r})}{\gamma} K_+^{\gamma,\mathrm{ss}}(\boldsymbol{1}, \ \boldsymbol{2}; \boldsymbol{r}) . \tag{D1}$$

We first rewrite the single-source definition of travel time (eq. [84]) in terms of the temporal Fourier transform of the signal observed at point $\boldsymbol{2}$:

$$\delta\tau_+^{\mathrm{ss}}(\boldsymbol{1}, \ \boldsymbol{2}) = -\frac{\mathrm{Re} \int_0^\infty d\omega \, i\omega \, \phi^{0*}(\boldsymbol{2}, \omega) \, \delta\phi(\boldsymbol{2}, \omega)}{\int_0^\infty d\omega \, \omega^2 |\phi^0(\boldsymbol{2}, \omega)|^2} . \tag{D2}$$

Given the pressure source $\rho\Theta$, located at point $\boldsymbol{1}$ and defined by equation (85), the zero- and first-order signals observed at $\boldsymbol{2}$ are

$$\phi^0(\boldsymbol{2}, \omega) = (2\pi)^4 \int_0^\infty k \, dk \, J_0(k\Delta) \mathscr{G}^{\Pi}(k, \omega) \Theta(k, \omega) , \tag{D3}$$

$$\delta\phi(\boldsymbol{2}, \omega) = (2\pi)^4 \, \Gamma^0(\omega) \int_{(A)} d\boldsymbol{r} \, \frac{\delta\gamma(\boldsymbol{r})}{\gamma} \int d\boldsymbol{k} \, d\boldsymbol{k}' \, e^{i\boldsymbol{k} \cdot \boldsymbol{\Delta}_1 - i\boldsymbol{k}' \cdot \boldsymbol{\Delta}_2} G^{\Pi}(\boldsymbol{k}, \omega) \, \Theta(\boldsymbol{k}, \omega) \, \hat{\boldsymbol{k}} \cdot \hat{\boldsymbol{k}}' \, \frac{\mathscr{G}^{\Pi}(\boldsymbol{k}', \omega)}{k'} . \tag{D4}$$

Using equation (D2) we obtain the damping kernel $K_+^{\gamma,\mathrm{ss}}$ in the form

$$K_+^{\gamma,\mathrm{ss}}(\boldsymbol{1}, \ \boldsymbol{2}; \boldsymbol{r}) = \frac{\int_0^\infty d\omega \, \omega^2 |\phi^0(\boldsymbol{2}, \omega)|^2 \mathscr{K}_+^{\gamma,\mathrm{ss}}(\boldsymbol{1}, \ \boldsymbol{2}; \boldsymbol{r}; \omega)}{\int_0^\infty d\omega \, \omega^2 |\phi^0(\boldsymbol{2}, \omega)|^2} , \tag{D5}$$

with the function $\mathscr{K}_+^{\gamma,\mathrm{ss}}$ (single-frequency kernel) defined by

$$\mathscr{K}_+^{\gamma,\mathrm{ss}}(\boldsymbol{1}, \ \boldsymbol{2}; \boldsymbol{r}; \omega) = \hat{\boldsymbol{\Delta}}_1 \cdot \hat{\boldsymbol{\Delta}}_2 \, \mathrm{Im}\left[\frac{\mathrm{IV}(\Delta_1, \omega) \, \mathrm{III}(\Delta_2, \omega)}{\omega \, \phi^0(\boldsymbol{2}, \omega)}\right] . \tag{D6}$$

In the above equation, the function IV is a one-dimensional integral given by

$$\mathrm{IV}(d,\omega) = (2\pi)^3 \Gamma^0(\omega) \int_0^\infty k\, dk\, J_1(kd) G^\Pi(k,\omega) \Theta(k,\omega) \,, \tag{D7}$$

and the function III denotes the integral already defined by equation (C13). Note from equation (D5) that the kernel $K_+^{\gamma,\mathrm{ss}}$ is a frequency average of $\mathscr{K}_+^{\gamma,\mathrm{ss}}$ weighted by $\omega^2 |\phi^0(\mathbf{2},\ \omega)|^2$.

In order to compute the kernel we have to make a choice for the source spectrum, $\Theta(k,\omega)$. In general, this is difficult without a priori knowledge of the zero-order cross-correlation. When comparing the definition of travel time of Appendix A with the single-source definition (eq. [84]), we find that a good match between the two definitions is obtained when $\phi^0(\mathbf{2},\ t)$ looks like $\mathrm{Hea}(t) C^0(\mathbf{1},\ \mathbf{2}, t)$. This condition is best met when

$$\Theta(k,\omega) = -\frac{k\, F(k,\omega)\, m^0(k,\omega)}{2\Gamma^0(\omega)} \,. \tag{D8}$$

Note that the filter function $F(k,\omega)$ appears in equation (D8). The kernel $K_+^{\gamma,\mathrm{ss}}$, shown in Figure 9, was computed using this choice.

REFERENCES

Birch, A. C., & Kosovichev, A. G. 2000, Sol. Phys., 192, 193
———. 2001, in Helio- and Asteroseismology at the Dawn of the Millennium, ed. A. Wilson (ESA SP-464; Noordwijk: ESA), 187
Birch, A. C., Kosovichev, A. G., Price, G. H., & Schlottmann, R. B. 2001, ApJ, 561, L229
Bogdan, T. J. 1997, ApJ, 477, 475
———. 2000, Sol. Phys., 192, 373
Bogdan, T. J., Braun, D. C., & Lites, B. W. 1998, ApJ, 492, 379
Bogdan, T. J., Brown, T. M., Lites, B. W., & Thomas, J. H. 1993, ApJ, 406, 723
Braun, D. C., Duvall, T. L., Jr., & LaBonte, B. J. 1988, ApJ, 335, 1015
Cally, P. S., & Bogdan, T. J. 1997, ApJ, 486, L67
Chou, D.-Y., LaBonte, B. J., Braun, D. C., & Duvall, T. L., Jr. 1991, ApJ, 372, 314
Christensen-Dalsgaard, J., Proffit, C. R., & Thompson, M. J. 1993, ApJ, 403, L75
Dahlen, F. A., & Tromp, J. 1998, Theoretical Global Seismology (Princeton: Princeton Univ. Press)
D'Silva, S., Duvall, T. L., Jr., Jefferies, S. M., & Harvey, J. W. 1996, ApJ, 471, 1030
Duvall, T. L., Jr., D'Silva, S., Jefferies, S. M., Harvey, J. W., & Schou, J. 1996, Nature, 379, 235
Duvall, T. L., Jr., & Gizon, L. 2000, Sol. Phys., 192, 177
Duvall, T. L., Jr., Jefferies, S. M., Harvey, J. W., Osaki, Y., & Pomerantz, M. A. 1993a, ApJ, 410, 829
Duvall, T. L., Jr., Jefferies, S. M., Harvey, J. W., & Pomerantz, M. A. 1993b, Nature, 362, 430
Duvall, T. L., Jr., Kosovichev, A. G., & Murawski, K. 1998, ApJ, 505, L55
Duvall, T. L., Jr., et al. 1997, Sol. Phys., 170, 63
Giles, P. M., Duvall, T. L., Jr., Scherrer, P. H., & Bogart, R. S. 1997, Nature, 390, 52
Gizon, L., & Birch, A. C. 2001, in Solar Encounter: The First Solar Orbiter Workshop, ed. B. Battrick & H. Sawaya-Lacoste (ESA SP-493; Noordwijk: ESA), 233
Gizon, L., Duvall, T. L., Jr., & Larsen, R. M. 2000, J. Astrophys. Astron., 21, 339
Gough, D. O. 1993, in Les Houches Session LXVII, Astrophysical Fluid Dynamics, ed. J.-P. Zahn & J. Zinn-Justin (Amsterdam: Elsevier), 399
Hung, S.-H., Dahlen, F. A., & Nolet, G. 2000, Geophys. J. Int., 141, 175

Jensen, J. M., Jacobsen, B. H., & Christensen-Dalsgaard, J. 1998, in Structure and Dynamics of the Interior of the Sun and Sun-like Stars, Vol. 2, ed. S. Korzennik & A. Wilson (ESA SP-418; Noordwijk: ESA), 635
———. 2000, Sol. Phys., 192, 231
Kosovichev, A. G. 1996, ApJ, 461, L55
Kosovichev, A. G., & Duvall, T. L., Jr. 1998, in SCORe'96: Solar Convection and Oscillations and their Relationship, ed. F. P. Pijpers, J. Christensen-Dalsgaard, & C. S. Rosenthal (Dordrecht: Kluwer), 241
Kosovichev, A. G., Duvall, T. L., Jr., & Scherrer, P. H. 2000, Sol. Phys., 192, 159
Kumar, P., & Basu, S. 2000, ApJ, 545, L65
Lamb, H. 1932, Hydrodynamics (6th Ed.; New York: Dover)
Lynden-Bell, D., & Ostriker, J. P. 1967, MNRAS, 136, 293
Marquering, H., Dahlen, F. A., & Nolet, G. 1999, Geophys. J. Int., 137, 805
Murawski, K., & Roberts, B. 1993, A&A, 272, 595
Nigam, R., & Kosovichev, A. G. 1999, ApJ, 514, L53
Saff, E. B., & Snider, A. D. 1993, Fundamentals of Complex Analysis for Mathematics, Science, and Engineering (2d Ed.; Upper Saddle River: Prentice Hall)
Sakurai, J. J. 1995, Modern Quantum Mechanics (Reading: Addison-Wesley)
Scherrer, P. H., et al. 1995, Sol. Phys., 162, 129
Stein, R. F. 1967, Sol. Phys., 2, 385
Stein, R. F., & Nordlund, A. 2000, Sol. Phys., 192, 91
Strous, L. H., Goode, P. R., & Rimmele, T. R. 2000, ApJ, 535, 1000
Tarbell, T. D., Acton, D. S., & Frank Z. A. 1997, in Adaptative Optics, Vol. 13, ed. D. Hennage (Washington: OSA), 96
Title, A. M., Tarbell, T. D., Topka, K. P., Ferguson, S. H., Shine, R. A., & The SOUP Team. 1989, ApJ, 336, 475
Tong, J., Dahlen, F. A., Nolet, G., & Marquering, H. 1998, Geophys. Res. Lett., 25, 1983
Vernazza, J. E., Avrett, E. H., & Loeser, R. 1981, ApJS, 45, 635
Woodard, M. F. 1997, ApJ, 485, 890
Woodward, M. J. 1992, Geophysics, 57, 15
Yaglom, A. M. 1962, An Introduction to the Theory of Stationary Random Functions (Englewood Cliffs: Prentice-Hall)
Zhao, L., & Jordan, T. H. 1998, Geophys. J. Int., 133, 683
Zhao, J., Kosovichev, A. G., & Duvall, T. L., Jr. 2001, ApJ, 557, 384